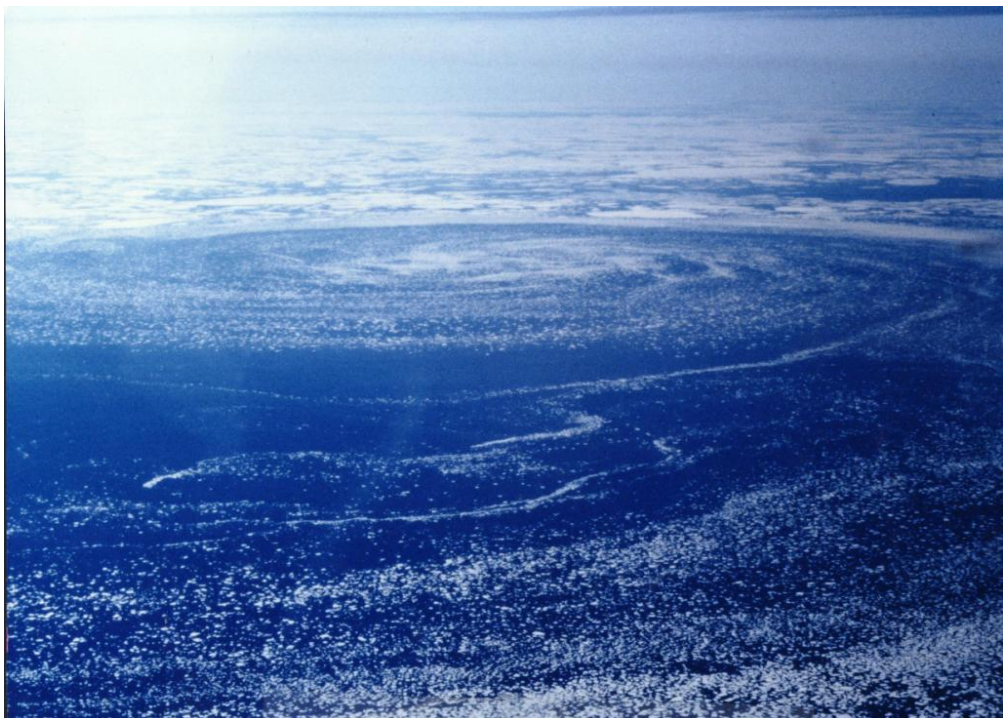


STUDIES OF EDDIES IN THE MARGINAL ICE ZONE  
ALONG THE EAST GREENLAND CURRENT USING  
SPACEBORNE SYNTHETIC APERTURE RADAR (SAR)



Thesis for the degree of Master in physical oceanography

ELIN BONDEVIK

JUNE 2011



UNIVERSITY OF BERGEN  
GEOPHYSICAL INSTITUTE



*The image on the front page: Aerial photography of a cyclonic ice edge eddy, taken at 79° N at 30th June, during MIZEX'84. The diameter of the eddy is approximately 40 km. The image is retrieved from Johannessen et al. (1987a).*

---

# Abstract

---

The characteristic ice edge eddies in the Marginal Ice Zone (MIZ) are studied based on satellite information from the Advanced Synthetic Aperture Radar (ASAR) instrument. The eddies frequency of existence during the day, month, and year, and their relationship to the wind field conditions are considered. On average, more than 1000 sea ice eddies were counted along the ice margin per year for 2008 and 2009.

Eddies contribute to an enhanced melting by forcing contact between the sea ice and the warmer water off the ice edge. The amount of sea ice an eddy can carry is estimated to be  $1413.7 \text{ km}^2$ . This constitutes  $0.7 \times 10^6$  by including the modified total of eddies during a year. The daily retreat of the ice edge is found to be  $3.5 \text{ km d}^{-1}$  per 100 km of ice edge. This estimation is based on the bottom ablation, radius of the eddy, distance between two neighbouring eddies, thickness of ice and fraction of sea ice trapped in an eddy.

The influence of the wind shows that relative low wind speed and wind directed from the north favours the existence of eddies.



---

# Acknowledgement

---

First of all, I would like to express my gratitude to my supervisor, Prof. Johnny Johannessen, for the support and constructive feedback, and for the possibility to work with a particularly interesting field of study. Thanks also to Knut-Frode Dagestad and Francois Counillon at NERSC for much appreciated input.

I am grateful to my family for the valuable support and for providing numerous time-offs with uplifting and motivating phone calls. The daily work has been memorable thanks to the friendly and cheerful group of fellow students at Odd and Høytrykket. At last, a special thanks to Erlend Moster Knudsen and Anniken Gjestad for the grammatical check.



---

# Table of Contents

---

<b>1</b>	<b>Motivation and Objectives</b>	<b>1</b>
<b>2</b>	<b>Background</b>	<b>5</b>
2.1	History . . . . .	5
2.2	The area . . . . .	6
2.2.1	Oceanographic conditions . . . . .	6
2.2.2	Bathymetry . . . . .	7
2.3	Eddy dynamics in the MIZ . . . . .	8
2.3.1	Characteristics . . . . .	9
2.3.2	Vorticity equation . . . . .	10
2.3.3	Ekman theory . . . . .	11
2.4	Eddy formation mechanisms . . . . .	13
2.4.1	Hydrodynamic instabilities . . . . .	13
2.4.2	Topography . . . . .	15
2.5	Eddy induced melting and the ice edge retreat . . . . .	16
2.5.1	Bottom and lateral melting . . . . .	17
2.5.2	Trapping of sea ice . . . . .	18
2.5.3	Calculation of the retreat . . . . .	19
<b>3</b>	<b>Data and Approach</b>	<b>21</b>
3.1	Remote sensing . . . . .	21
3.1.1	The Satellite . . . . .	22
3.1.2	Advanced SAR (ASAR) . . . . .	24
3.2	Principles of SAR . . . . .	24
3.2.1	Resolution in azimuth and range . . . . .	25
3.2.2	Scattering . . . . .	26
3.3	SAR image interpretation . . . . .	27
3.3.1	Eddy signature . . . . .	28

3.4	Wind retrieval . . . . .	29
<b>4</b>	<b>Results</b>	<b>33</b>
4.1	Statistics of eddy occurrence . . . . .	33
4.1.1	Monthly variability . . . . .	33
4.1.2	Regional variability . . . . .	37
4.2	Size . . . . .	38
4.2.1	The amount of sea ice trapped in the eddy . . . . .	39
4.3	Wind influence . . . . .	40
4.4	Retreat of the ice edge . . . . .	47
<b>5</b>	<b>Discussion</b>	<b>53</b>
5.1	Regional and seasonal variation . . . . .	53
5.2	Wind influence . . . . .	56
5.3	Eddy cyclones versus anticyclones . . . . .	59
5.4	The eddy induced melting . . . . .	60
<b>6</b>	<b>Conclusion</b>	<b>63</b>
<b>A</b>	<b>Abbreviations</b>	<b>67</b>
<b>B</b>	<b>Data</b>	<b>69</b>
B.1	The Data from 2008 . . . . .	69
B.2	The Data from 2009 . . . . .	76
	<b>References</b>	<b>83</b>



# CHAPTER 1

---

## Motivation and Objectives

---

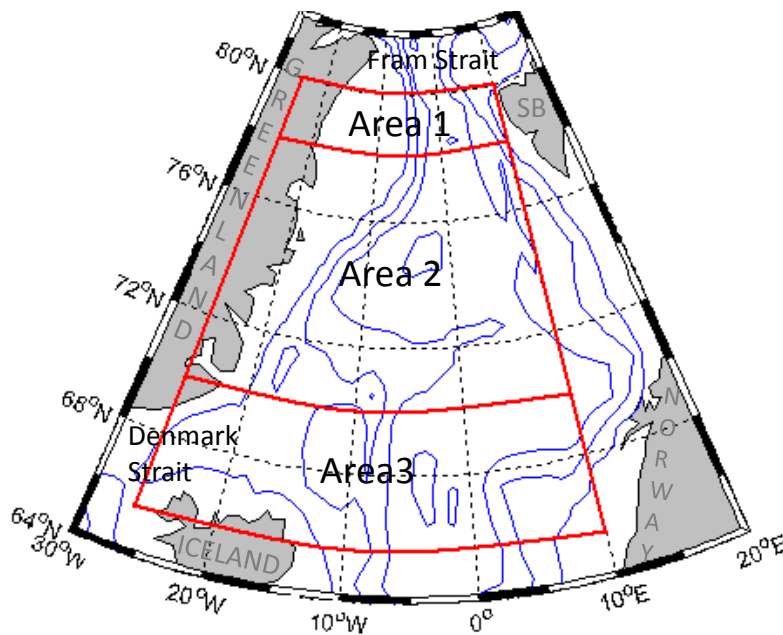
In this thesis, mesoscale eddies in the Marginal Ice Zone (MIZ) and their contribution to melting of sea ice are investigated using satellite based Synthetic Aperture Radar (SAR). The hypothesis is that eddies advect warm water closer to and beneath the sea ice, and sweep ice away from the ice edge into warmer water. Eddies also contribute to a nonuniform ice motion that leads to ice deformation and more open water, which enhances the melting potential.

The melting is accelerated because of these processes (Johannessen *et al.*, 1987a,b; Manley, 1987; Quadfasel *et al.*, 1987; Vinje & Finnekåsa, 1986), but the magnitude of the melting remains unknown. The motivation of this thesis with the goal *to examine the role of eddies for the melting of sea ice* capitalizes on this. Essential information needed to achieve this goal is how much ice an eddy can carry and how effective the eddy can melt this ice. In addition, the total number of eddies in the region, both seasonal and annual, are needed to determine the full effect. A two-year period of data is chosen to obtain this information; from 1st January 2008 to 31st December 2009.

The smallest length scale of a mesoscale eddy is determined by the Rossby radius of deformation. Here, a mesoscale eddy is defined to have a radius between 20-40 km. This is a relative small spatial scale, and by adding that the lifetime of an eddy is 20-30 days, regular *in-situ* measurements are challenging to obtain. Remote sensing overcomes these limitations, using SAR.

The area of interest is the MIZ in the Fram Strait, Central and East Greenland

Sea and the Denmark Strait, named Area 1, Area 2 and Area 3, respectively (*cf.* Figure 1.1). The MIZ, defined as the zone between the open ocean and the ice-covered area, is a key area for interactive processes between air, sea and ice (Johannessen *et al.*, 1987b). Eddies are found almost everywhere they have been looked for (Robinson, 1983), but the role of eddies in the MIZ is particularly intriguing because they also affect the sea ice deformation and melting, as suggested by Johannessen *et al.* (1987b). Eddies alter the current structure of the two characteristic water masses in the area; the warm Atlantic Water (AW) and cold Polar Water (PW), thus enabling the melting.



**Figure 1.1:** The study area, divided in three parts: Area 1 between  $78-80^\circ$  N (the Fram Strait), Area 2 between  $70-78^\circ$  N (Central and East Greenland), and Area 3 between  $65-70^\circ$  N (the Denmark Strait). The western boundary is at  $25^\circ$  W, the eastern is at  $10^\circ$  E. (SB represents Svalbard)

The presence of sea ice plays a pivotal role when it comes to the world's climate, and changes in sea ice concentration, extent and thickness are leading indicators of climate change (Thomas & Dieckmann, 2003). Melting of sea ice leads to more freshwater (since the ice is relatively fresh) and modifies the freshwater flux out of the Greenland Sea. This may affect the thermohaline ocean circulation and formation which in turn can influence the entire climate (Thomas & Dieckmann, 2003). Any modification of the sea ice extent will therefore have an impact on both regional and global climate.

When looking at the Earth system from an even wider perspective; the sea ice

---

cover affects the Earth's radiation budget, the surface heat exchange and albedo<sup>1</sup>. The presence of sea ice reduces the heat and momentum exchange between the ocean and the atmosphere. The surface heat loss is reduced by 1-2 orders due to the presence of sea ice (Maykut, 1978). The albedo of ice is higher (between 0.5-0.85, depending on the age of the ice) than the dark, open sea (albedo about 0.1 or lower, depending on the sun-angle) (Thomas & Dieckmann, 2003). More solar radiation will be absorbed in regions with less ice compared to the ice covered areas. This results in more ice melting, which leads less ice cover, that also result in more solar absorption. This is known as a positive feedback.

The increased melting is not the only intriguing result of eddies in the ocean. They control the horizontal mixing and are in that sense an essential element in various special fields. Eddies have a special dynamic with important influence on biological, chemical and physical conditions, and knowledge about the physical science of eddies gives important information about the other two sciences (Robinson, 1983). Eddies are also suggested being a contributor to the recent warming of the Arctic Ocean, by modifying the inflow through the Bering Strait (Maslowski *et al.*, 2008).

In Chapter 2, some history of eddy experiments and general information about the area are presented, together with existing dynamical theories and eddy formation mechanisms. The theory around the data acquisition and the method used to extract the relevant data are summarized in Chapter 3. After analysis and presentation of the results in Chapter 4, the discussion follows in Chapter 5. Some concluding remarks are made in Chapter 6. The definitions of the abbreviations are listed in Appendix A, and the gathered and used data can be found in Appendix B.

---

<sup>1</sup>The percentage of incoming radiation that is reflected.



# CHAPTER 2

---

## Background

---

### 2.1 History

Eddies in the ocean were noted by navigators in early time, but were not fully documented until the end of the 1970s and the early 1980s. Exploration of the ocean became more clearly set out after the first satellite was launched in 1957. This made a considerable contribution to oceanography; the possibility to observe the ocean from space has revealed various phenomena that would be difficult to detect otherwise. In addition, the opportunity to collect synoptic data over large areas became available. The first time the spiraling eddies in the ocean were manifested in a photograph was in October 1968, captured by the astronauts on the Apollo Mission (Munk *et al.*, 2000). Investigation of eddies started with the POLYGON-70, Mid-Ocean Dynamics Experiment (MODE-1) in 1973 and the Polygon Mid-Ocean Dynamics Experiment (POLYMODE) in 1979 (Robinson, 1983). Approximately ten years after the first eddies were seen in the photograph, the first satellite (SEASAT) with SAR was launched by the National Aeronautics and Space Administration (NASA). Eddy investigation reached its peak during the 1980s. In the Arctic region, three extensive experiments were made, documented as the Marginal Ice Zone Experiments (MIZEX). The first was made in the summer of 1983 where physical and exchange processes around mesoscale eddies were in focus. The larger follow-up was made in 1984. Well-documented investigations were made; data were obtained from satellite, aircraft, ship taken

conductivity-temperature-depth (CTD) sections, floats and current meters (Johannessen *et al.*, 1987a; Josberger, 1987; Sandven *et al.*, 1991). The third experiment, MIZEX'87, was a winter experiment focusing on the deep water formation and its relation to the mesoscale eddies (Sandven *et al.*, 1991).

## 2.2 The area

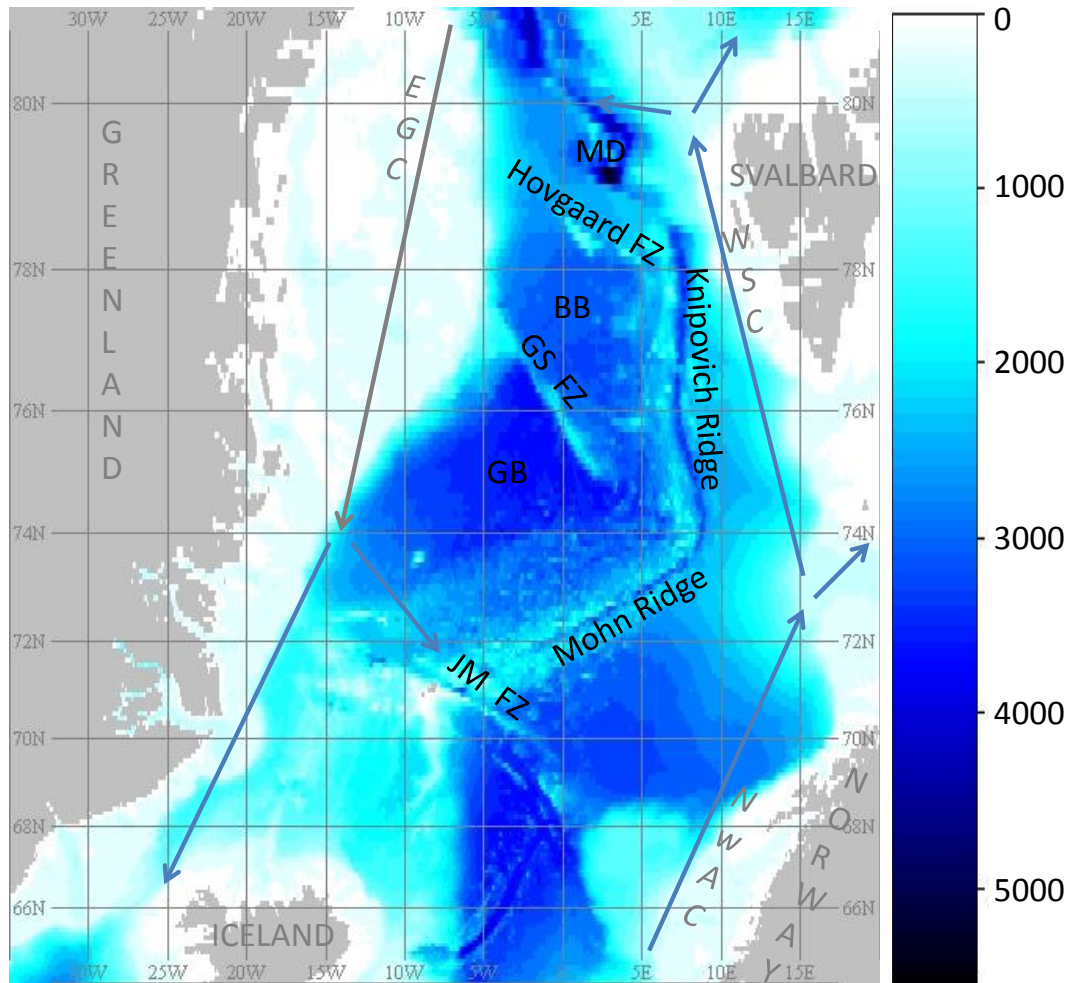
### 2.2.1 Oceanographic conditions

The Fram Strait, a 600 km wide passage between Svalbard and Greenland, represents a unique deep water connection between the Arctic Ocean and the rest of the world oceans. The two main currents that control the water mass exchange are the West Spitsbergen Current (WSC) and the East Greenland Current (EGC) (Carmack, 1990). The rough location of the currents are shown in Figure 2.1.

The WSC is an extension of the Norwegian Atlantic Current (NwAC), flowing northward through the Fram Strait along the west coast of Svalbard. It separates into filaments that either recirculate in the Fram Strait and continues southward with the EGC, or continues northward into the Arctic Ocean. It carries relatively warm and saline AW (Atlantic Water), and is the dominant heat and salt source for the Arctic Ocean, with a characterized temperature above 3° C and salinity above 35 (Quadfasel *et al.*, 1987). The WSC transports on average 5.6 SV (1 SV =  $1 \times 10^6 \text{ m}^3 \text{ s}^{-1}$ ) of AW, and carries about 40 TW (1 TW =  $10^{12} \text{ W}$ ) of heat northward each year (Hanzlick, 1983).

The EGC is the southward flowing current in the area, following the east coast of Greenland. It carries large amounts of ice in addition to cold (usually below 0° C) and fresh PW (Polar Water). It transports 2-3 SV (Aagaard & Coachman, 1968), and removes annually between 4000-5000 km<sup>3</sup> of both multi-year (MY) and first-year (FY) ice (Vinje & Finnekåsa, 1986). When the wind is directed south-westward along the East Greenland coast, the sea ice reaches a maximum speed at the ice edge. This phenomenon is known as an ice edge jet (Johannessen *et al.*, 1983).

The EGC is described as a narrow jet that is dynamically stable and strongly coupled with topography. The WSC, on the other hand, is naturally unstable, and has a profusion of open ocean eddies (Gascard *et al.*, 1988). These characteristics are of interest when it comes to the subject of generation mechanisms.



**Figure 2.1:** *The bathymetry and the two main currents of the area. BB = Boreas Basin, GB = Greenland Basin, GS = Greenland Sea, JM = Jan Mayen and FZ = Fracture Zone. The currents: EGC = East Greenland Current and WSC = West Spitsbergen Current. The bathymetric data are retrieved from General Bathymetric Chart of the Oceans (GEBCO) (BODC, 2010), the current data from Carmack (1990).*

### 2.2.2 Bathymetry

The map in Figure 2.1 covers the bathymetry of the area. The largest variation in the bathymetry occurs in the Fram Strait, where depressions, sea mounts and ridges exist. The maximum depth extends to 5500 m below the surface, known as the Molloy Deep, which is recognized as the dark blue area at approximately 79° N. The sea mounts and ridges rise steeply to 1500 m below the surface.

The Greenland Sea is divided in two main basins, the Boreas Basin (BB) and the Greenland Basin (GB), which of the latter is deeper. The basins have a depth

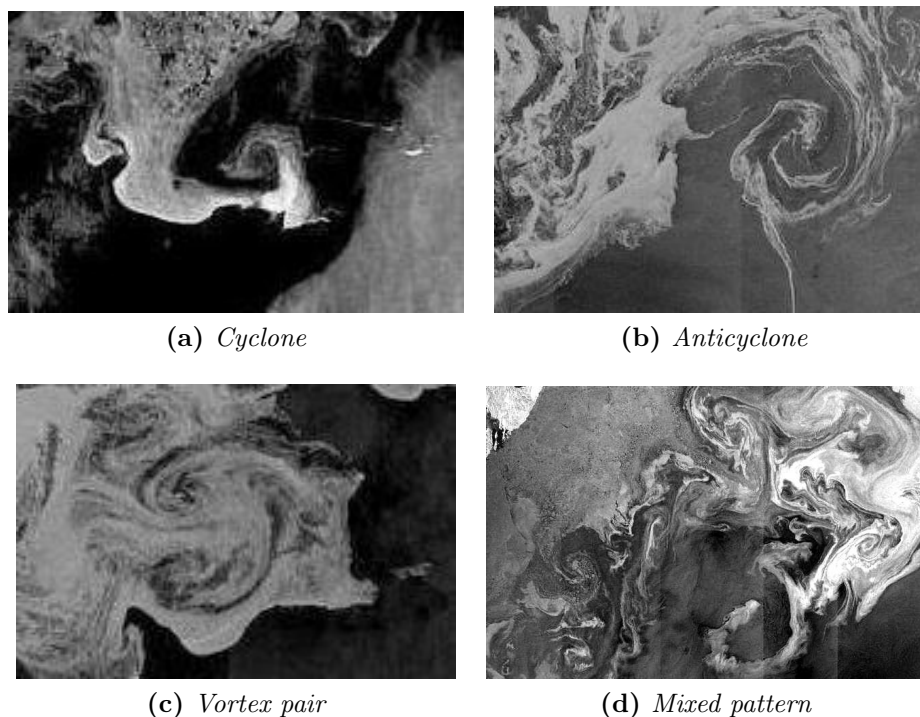
around 3200-3800 m and are surrounded by ridges and continental shelves. To the north, the BB is closed by the Hovgaard Fracture Zone, situated between 78-79° N and around 0° E. The Knipovich mid-ocean ridge is the eastern boundary, and the continental shelf borders the west side. The Greenland Sea Fracture Zone is the boundary between the BB and GB. The Mohn ridge closes the GB on the eastern side. To the west, the continental shelf exists, in the south Jan Mayen and the Jan Mayen Fracture Zone makes a boundary.

The depth decreases in the area west and south-west of Jan Mayen. The northern part of the Denmark Strait is characterized by the form of a v-shaped sill, with continental shelves as borders at each side. Note that the complex bathymetry may impose equally complicated topographic steered currents.

## 2.3 Eddy dynamics in the MIZ

An eddy is defined as a relative persistent closed circulation. With that it is implied that the time it takes for a fluid parcel to complete one turnaround is much shorter than the time the structure is traceable at the surface (Cushman-Roisin & Beckers, 2009). The rotational direction decides if the eddy is termed a cyclone or an anticyclone; a cyclone is a vortex with rotational motion in the counter clockwise direction in the Northern Hemisphere (NH) (clockwise in the Southern Hemisphere (SH)), an anticyclone rotates clockwise in the NH (counter clockwise in the SH). An example of a cyclone (from the NH) can be seen in Figure 2.2a, Figure 2.2b shows an anticyclone. Other patterns that can be found in the MIZ comprise vortex pair and mixed pattern. A vortex pair, also called the mushroom-like pattern, consists of both a cyclone and an anticyclone, as Figure 2.2c shows. A mixed pattern is more chaotic, with all the three mentioned patterns included, as in Figure 2.2d.





**Figure 2.2:** Four ASAR images that reveal eddy signature. A cyclone can be seen in (a), an anticyclone in (b), a vortex pair in (c) and at last an image with a mixed pattern (d). The diameters are about 40 km of the cyclone, 45 km of the anticyclone approximately 50 km of the vortex pair, and about 100 km for the whole area in (d), respectively. All images are taken in the MIZ in the NH.

### 2.3.1 Characteristics

The dominant forces regarding the eddy dynamics are usually covered by Equation 2.1, known as the *gradient-wind balance*. It represents an equilibrium between three forces; the centrifugal force ( $-v^2/r$ ), the Coriolis force ( $-fv$ ) and the pressure force ( $-\rho_0^{-1}\partial p/\partial r$ ),

$$-\frac{v^2}{r} - fv = -\frac{1}{\rho_0} \frac{\partial p}{\partial r} \quad (2.1)$$

$v$  is here the azimuth velocity (positive counter clockwise),  $r$  the radius of the eddy,  $\partial/\partial r$  the derivative along  $r$ ,  $f$  the Coriolis parameter, and  $p$  is the pressure. If  $r \rightarrow \infty$ , the centrifugal term becomes negligible, thus the geostrophic balance is retrieved (Cushman-Roisin & Beckers, 2009).

If the Coriolis force dominates over the centrifugal force, the eddy is termed quasi-geostrophic. In the opposite case, the eddy is non-linear. The Rossby number

normally represents this classification, by comparing advection to the Coriolis force,

$$R_0 = \frac{g'H}{f^2 L^2} = \left(\frac{R_d}{L}\right)^2 \quad \text{with} \quad R_d = \frac{\sqrt{g'H}}{f} \quad (2.2)$$

Here,  $R_0$  is the Rossby number. It characterizes the importance of rotation in a fluid, the effect of rotation is opposite proportional to this number.  $H$  [m] is the depth of the mixed layer,  $f$  [ $\text{s}^{-1}$ ] is the Coriolis parameter and  $L$  [m] is the typical width of the domain.  $g'$  [ $\text{m s}^{-2}$ ] is the reduced gravitation, defined as  $g' = (\Delta\rho/\rho_0)g$  (where  $\Delta\rho$  [ $\text{kg m}^{-3}$ ] is the difference in density between the two layers,  $\rho_0$  is the density of the lower layer, and  $g$  [ $\text{m s}^{-2}$ ] is the effect from gravitation). If  $R_0 \sim O(1)$ , the eddy is non-linear, while if  $R_0 \ll 1$ , the eddy termed quasi-geostrophic.

In Equation 2.2,  $R_d$  is the Rossby radius of deformation. It represents the minimum size of an eddy. The length scale is determined by the speed of a baroclinic gravity wave divided by the natural time scale of the Coriolis parameter ( $f$ ). Dynamical structures that are smaller than this radius will either evolve to larger structures (with a radius  $>R_d$ ), or they will propagate away. Structures with length scale bigger than the deformation radius are expected to be in geostrophic balance.

The structure is also bounded by the upper end, since  $f$  varies with latitude ( $\beta$ -effect). The Coriolis parameter is zero at the equator and increases towards a maximum at the poles. The tendency of a disturbance in a current to move in a curved pattern increases therefore with the distance from equator (Brown *et al.*, 2001).

### 2.3.2 Vorticity equation

To describe the physical nature of eddies, the relative vorticity and the equation for change in vorticity are introduced. Vorticity quantifies the rotation rate of a fluid. The intensity of the vorticity is given as

$$\zeta = \frac{\partial v}{\partial x} - \frac{\partial u}{\partial y} \quad (2.3)$$

where  $\zeta$ , known as the relative vorticity, is defined as  $\nabla_z \times \mathbf{u}$  ( $\mathbf{u} = (u, v)$ ). The

vorticity equation, retrieved from Kundu (1990), is of importance when considering the formation mechanisms, both when it comes to the contribution from topography and the hydrodynamic modulations. The equation is given as

$$\frac{D}{Dt}(\omega) = (\mathbf{f} + \omega) \cdot \nabla \mathbf{u} \beta \mathbf{v} + \frac{1}{\rho^2} \nabla \rho \times \nabla \mathbf{p} + \nu \nabla^2 \omega \quad (2.4)$$

where  $\omega$  is defined as  $\nabla \times \mathbf{u}$ . The left side of the equation represents the modification of the vorticity following a fluid parcel. The first term on the right side represents the contribution from stretching of the vorticity gradients. The second term of the equation,  $\rho^{-2}(\nabla \rho \times \nabla p)$ , is the baroclinic contribution to a material change of vorticity. The third term is a measure of the diffusion of the vorticity due to frictional properties of the fluid.

### 2.3.3 Ekman theory

Vagn Walfrid Ekman developed a theory covering the effect of wind stress on the ocean surface. A horizontal frictional stress takes place on the surface in relation to the wind force. A moderate surface stress may generate large drift velocities if the fluid is close to inviscid. Cushman-Roisin & Beckers (2009) presents the theory more thoroughly, here it is focused on the essentials. The wind-driven horizontal components of the transport in the surface Ekman layer are given as

$$U = \int_{-\infty}^0 (u - \bar{u}) dz = \frac{1}{\rho_0 f} \tau^y \quad (2.5a)$$

$$V = \int_{-\infty}^0 (v - \bar{v}) dz = -\frac{1}{\rho_0 f} \tau^x \quad (2.5b)$$

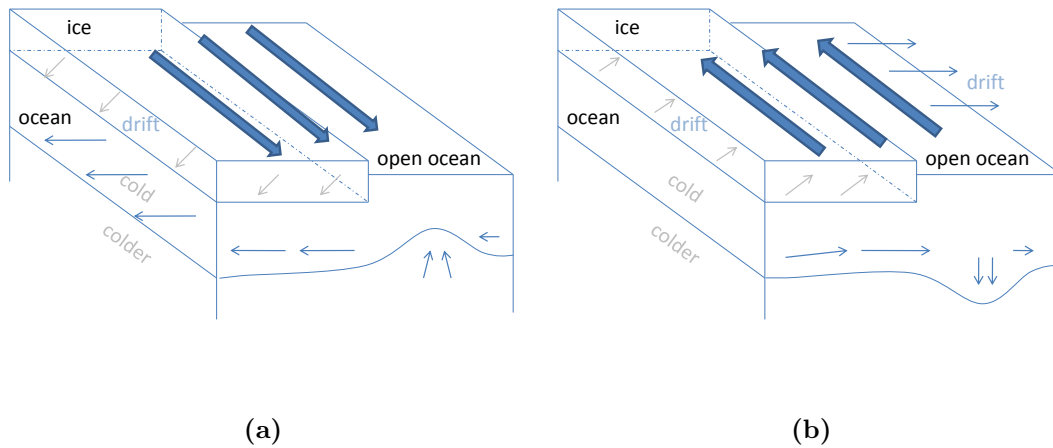
Here,  $u$  and  $v$  are the flow field,  $\bar{u}$  and  $\bar{v}$  are the interior flow field,  $\rho_0$  is the density and  $f$  is the Coriolis parameter.  $\tau^y$  and  $\tau^x$  are the wind stress components, defined as

$$\tau^x = C_d \rho_a U u, \tau^y = C_d \rho_a U v \quad (2.6)$$

where  $U = \sqrt{u^2 + v^2}$  is the wind speed,  $u$  and  $v$  are the  $x$  and  $y$  components of the wind vector, respectively, and  $\rho_a$  is the density of air.

By inserting the components of Equation 2.5 in  $V = \int_0^\infty v dz$ , the perpendicular

relationship between the wind stress and the wind driven horizontal transport in the NH (oppositely in the SH) is evident: With a wind directed from north, Lagrangian drifters<sup>1</sup> in a current will be forced towards the west ( $90^\circ$  to the right). A sketch of this event can be seen in Figure 2.3a. With a wind blowing from the south the drifters are forced towards the east (Figure 2.3b). This theory is of interest when focusing on the subject of how eddies disappear, and it plays a crucial role when it comes to the visibility of eddies at the surface.



**Figure 2.3:** *The direction of the wind (blue arrows) and the resulting Ekman transport (grey arrows); with wind from north (a) and wind from south (b). The appurtenant ice edge drift and the resulting upwelling or downwelling in the two situations are also evident. The figures are based on Cushman-Roisin & Beckers (2009, Figure 15-6)*

The drag coefficients,  $C_d$  (from Equation 2.6), depend on the surface characteristics. For water,  $C_{d,aw}$  has a magnitude of  $1.2 \times 10^{-3}$ , while over ice,  $C_{d,ai}$  has a magnitude of  $3.6 \times 10^{-3}$  (the subscripts  $a$ ,  $w$  and  $i$  are for air, water and ice, respectively). Generally  $C_{d,ai}$  is 2-3 times greater than the drag coefficient of air and water, ( $C_{d,aw}$ ) (Häkkinen, 1986). This means that the wind experiences more stress over sea ice than water, which results in uneven movement of the sea ice compared to the water. This may generate upwelling or downwelling, the outcome depends on the direction of the wind, as seen in Figure 2.3a and 2.3b.

<sup>1</sup>Drifters designed to follow a current, ocean front, river flows etc.

## 2.4 Eddy formation mechanisms

Johannessen *et al.* (1987a) identified five sources that are capable of generating eddies; barotropic and baroclinic instabilities, topography, advected eddies from the WSC and external forcing. The following section is mostly based on their findings, but the dynamical part is based on Cushman-Roisin & Beckers (2009); Kundu (1990) and Pedlosky (1987). It should be noted that an eddy may be generated by a mixture of the sources suggested.

Two of the generation mechanisms mentioned are of minor importance, and will be just briefly summarized. The first is the theory covering the advected eddies. It has been suggested that eddies are not produced locally in the EGC, instead observations indicate that eddies are advected from the WSC (Smith & Bird, 1991). Parts of the AW in the WSC are recirculated in the Fram Strait, and open ocean eddies in the AW are advected towards the MIZ; an interaction that may lead to ice edge eddies. As the AW is forced beneath the PW (due to higher density), the relative distance between the isopycnals increase, and the relative vorticity must increase equally. The other generation mechanism is related to the Ekman transport described in Section 2.3.3. The coupling air-ice-water is stronger than the air-water coupling, resulting in different Ekman transport. The wind along an ice edge might result in eddy formation in response to the varying ice cover and meandering structure of the ice edge (Häkkinen, 1986).

### 2.4.1 Hydrodynamic instabilities

In the frontal zone of the EGC, barotropic and baroclinic processes combine to form mesoscale eddies. The instability phenomena are closely linked to the transfer of energy from the mean flow to the eddy kinetic part.

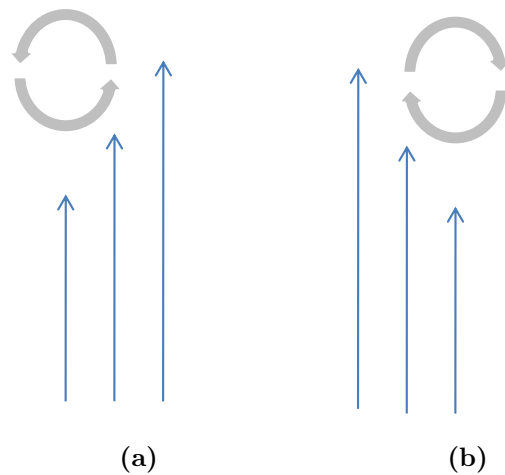
#### Barotropic instability

A barotropic region is a region with a well-mixed (thus homogeneous and non-stratified) water mass. The density of the water will increase with depth, an attribute of barotropy is that the pressure is a function of density only ( $p = p(\rho)$ ), and vice versa. The isobaric and the isopycnic surfaces will thus be parallel.

Barotropic instability is known as a shear instability due to its dependency on the horizontal shear of the current;  $\partial u/\partial y, \partial v/\partial x$ . The vorticity is generated

by the shear flow. A criterion for this instability is that an inflection point in the horizontal current profile must exist somewhere in the flow, as in Figure 2.4 (Pedlosky, 1987). The sign of the shear state the rotational direction.

By looking at the vorticity equation (Equation 2.4) for a barotropic fluid, it is evident that the second term on the right hand side is zero, since  $\nabla\rho \times \nabla p = 0$ . This demonstrates that barotropic fluids does not make a contribution to the change in vorticity.



**Figure 2.4:** *The idealized velocity shear and the corresponding direction of the eddy motion due to the barotropic instability. Cyclonic rotation is the result in (a), anticyclonic rotation in (b).*

### Baroclinic instability

In a baroclinic fluid the pressure is not a function of density alone, it is dependent on density and temperature ( $p = p(\rho, T)$ ). The isobaric and isopycnic surfaces are not parallel at all depths, as apposed to the barotropic case. A vertical shear thus exists, which also implies horizontal density gradients. These gradients can store available potential energy because of the inclined density surfaces, since a system with inclined density surfaces has more potential energy than a system where the density surfaces are horizontal. The release of this potential energy may generate eddies.

In the vorticity equation (Equation 2.4), the second term on the right hand side will provide a contribution to the change in vorticity. More thorough theory about baroclinic and barotropic instabilities can be found in Kundu (1990); Pedlosky (1987).

The characteristics of a density driven coastal current bounded by a front were investigated by Griffiths & Linden (1982) by the use of a laboratory experiment. The result was that a comparison between the Rossby radius of deformation and the width of the current could reveal if the current was barotropic or baroclinic. They concluded that if the current width is comparable to the Rossby radius of deformation (Equation 2.2), the length scale of disturbances and the width of the current are proportional. But if the upper layer is much wider, the observed length scale is a constant multiple of the Rossby radius. From this, Griffiths & Linden (1982) concluded that if the current width is about the same size as the Rossby radius of deformation, the instability will be barotropic. On the other hand, if the horizontal scale of motion is much bigger than the deformation radius, the instability is classified as baroclinic.

### 2.4.2 Topography

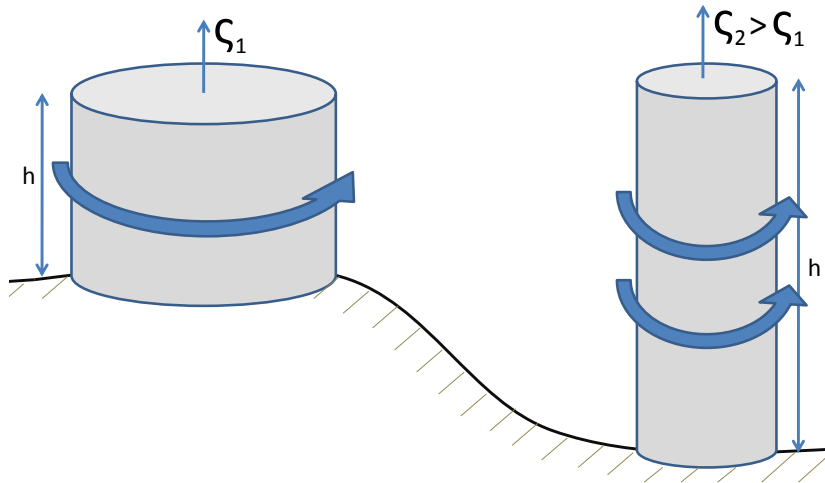
To consider the effect of bathymetric variations on the fluid boundary, the use of potential vorticity is useful. The shallow-water model (which one can read more about in e.g. Cushman-Roisin & Beckers (2009); Kundu (1990); Pedlosky (1987)) is used to obtain the equation for conservation of potential vorticity,

$$\frac{D}{Dt} \left( \frac{\zeta + f}{h} \right) = 0 \quad (2.7)$$

$(\zeta + f)$  is defined as the absolute vorticity,  $\zeta$  is the relative vorticity (Equation 2.3) while  $f$  is the planetary vorticity (the effect of Earth's rotation). The potential vorticity ( $q$ ) is defined as  $(\zeta + f)/h$ , where  $h$  is the thickness of the density layer.

Equation 2.7 states that the vorticity is conserved. When a fluid parcel moves over an area of increasing depth, the vorticity must increase (producing more cyclonic motion). When it moves over an area with decreasing depth ( $h$ ) the fluid parcel will be compressed and lead to more anticyclonic rotation. This is illustrated in Figure 2.5.

Proudman (1916) and Taylor (1917) calculated the generation of eddies due to an interaction between topography and an ocean current, and they suggested anticyclonic eddies over a sea-mount and cyclonic eddies over a depression. To confirm this, a detailed study of the Molloy Deep area was conducted during MIZEX'84. Deep CTD observations revealed that the eddy-signature extends all the way down to the bottom, and the topography as a generation mechanism was



**Figure 2.5:** *The volume and vorticity of a fluid parcel are conserved when moving over varying bathymetry, in accordance with Equation 2.7.  $h$  is the thickness of the density layer,  $\zeta_1$  and  $\zeta_2$  are the vorticity.*

with that verified (Johannessen *et al.*, 1987a).

An eddy may be trapped or steered off a topographic feature, Huppert & Bryan (1976) used an equation to answer the fate of an eddy generated by topography: If  $(Nh_m)/U_0$  is of  $O(10^1)$ , the eddy generated by the bathymetry is trapped. But if the equation is of  $O(10^0)$ , the eddy may be shed off. The equation is the inverse Froude number<sup>2</sup> where  $N$  is the Brunt-Väisälä frequency,  $h_m$  is the height of the bathymetric feature and  $U_0$  is the mean flow velocity. For the eddy generated in the Molloy Deep area that was investigated by Smith *et al.* (1984), one may find the size of the parameters for the equation. It is used that  $U_0$  is  $0.1 \text{ m s}^{-1}$ ,  $h_m$  is 1000 m and  $N$  is of  $O(10^{-3}) \text{ s}^{-1}$ . This gives a value of  $O(10^1)$ , which means that the eddy must remain trapped. In occasions with strong pulsations of the mean current, the number may cease towards 2. This enables the possibility for eddies to propagate.

## 2.5 Eddy induced melting and the ice edge retreat

The eddies are known to sweep ice and PW off and advect warm AW closer to the ice edge. The amount of sea ice trapped in an eddy and the thickness of this

<sup>2</sup>A dimensionless number that determines an objects resistance of moving through water.



ice are the two quantities of importance when working with the eddy induced melting. Before this subject is contemplated, the contact between sea ice and the warmer water is considered.

### 2.5.1 Bottom and lateral melting

The mentioned contact between the sea ice and warmer water accelerates the ice ablation. The vertical melting of sea ice is in response to an imbalance between heat fluxes at the boundaries and internal conduction of heat. An ice floe is in contact with the ocean on the bottom and the lateral surfaces. Bottom ablation was investigated by Josberger (1987) as a part of the MIZEX. The melt rate was measured by acoustic bottom ablation gauges, which measure the distance between the overlying ice and acoustic transducer below the ice. Periodic measurements ensure that the subsequent change in this distance becomes apparent, and thereby exposing the melt rate. The relative ice-water velocity, salinity and temperature were measured simultaneously at 2 and 10 meters below the ice floes. The minimum melt rate is given as  $0.25 \text{ m d}^{-1}$ , but rates as high as  $0.5 \text{ m d}^{-1}$  were also measured. The difference in bottom melt rates are mainly due to the relative speed between the ice and the water, and the temperature. If the relative velocity is large, the melting is enhanced. The salinity is fairly constant in the area. On a time scale of a few days, the oceanographic conditions within a few meters of the ice control the bottom ablation directly.

The lateral sides of an ice floe also absorb heat from the open water. In the article by Hall & Rothrock (1987), one can read about the use of photogrammetry to measure the lateral melting. The experiment was made during MIZEX'83-84. The technique involves photographs of a chosen ice floe two separate days, and the changes in the floe boundary are calculated. The lateral melt rate was measured to be as high as  $0.1 \text{ m d}^{-1}$ , but melt rates of  $0.02 \text{ m d}^{-1}$  were more commonly observed. Lateral melting are influenced by a number of different mechanisms that one can read more about in Steele & Flato (2000, and references therein). They conclude that lateral melting is significant only for floes less than several hundred metres in diameter.

Lateral ablation gain influence when the size of the ice floe decrease. This is argued by scaling the area of the bottom versus the lateral area. The bottom area of a circular ice floe is  $\pi r^2$ , while the area of the lateral sides is  $2\pi rh$ , where  $r$  is the radius and  $h$  is the thickness of the ice. The circumference can become

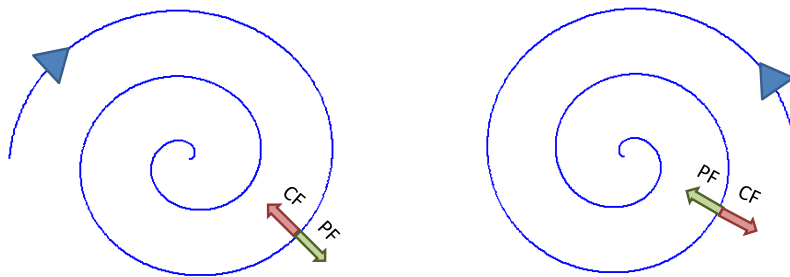
comparable to the area as the radius of the ice floe decreases. This is because the ratio of lateral area to bottom area is greater for small ice floes than for large ice floes.

### 2.5.2 Trapping of sea ice

The melting potential is distributed over a wider area due to the eddies' non-uniform motion. Moreover, this dilution will gradually make the sea ice structurally weak, which makes the ice more sensitive to collisions between ice floes, thus accelerating the melting even more (smaller ice floes melt away faster than the larger ice floes). The trapping of sea ice in the centre of the eddy is an interesting and a vital property of eddies, and the amount of ice trapped is crucial when working out their effect on melting.

The ice is transported towards the centre of the eddy by means of the spiraling motion. This is illustrated by Figure 2.6. One can imagine sea ice in the spirals to understand that the motion simply transports the sea ice towards the centre, where it also remains trapped because of the same motion.

The spiraling lines might be evidence of ageostrophic motion. The ageostrophy ensures that the sea ice will gather in the centre of an anticyclonic eddy (convergence), while dispersion is a more likely effect in the cyclones (divergence). It is thus expected that anticyclones contain more sea ice. The frictional inward radial motion is assumed to be the effect at work, but also the resulting surface tilt may have an affect (Johannessen *et al.*, 1987a).



**Figure 2.6:** *This schematic illustration suggests how ice is transported towards the centre. The balance of the pressure (gradient) force (PF) and the Coriolis force (CF) resulting in geostrophic balance is also included.*

### 2.5.3 Calculation of the retreat

The zonal retreat of the ice edge is a good indicator of the effect of eddies. The average retreat of the ice edge can be estimated with the help from Equation 2.8, following Johannessen *et al.* (1987a):

$$A = \frac{w\pi r^2}{2lh} \quad (2.8)$$

Where  $w$  [ $\text{m d}^{-1}$ ] is the bottom ablation given by Josberger (1987). The eddy is assumed to be circular, so the area of the eddy can be set to  $\pi r^2$ , where  $r$  [km] is the radius of the eddy. The distance between the centres of two eddies are given by  $l$  [km], to cover the effect of eddy-eddy interaction.  $h$  [m] is the thickness of the ice. The scaling factor by 2 is due to the fact that the eddy normally contains 50 % of ice.  $A$  [ $\text{m d}^{-1}$ ] express the average retreat of the ice edge (with the distance  $l$ ).

The sea ice volume in an eddy can be calculated using the formula for volume of a cylinder ( $\pi r^2 h$ ), where  $h$  is the thickness of the ice and  $r$  is the radius of the eddy.



# CHAPTER 3

---

## Data and Approach

---

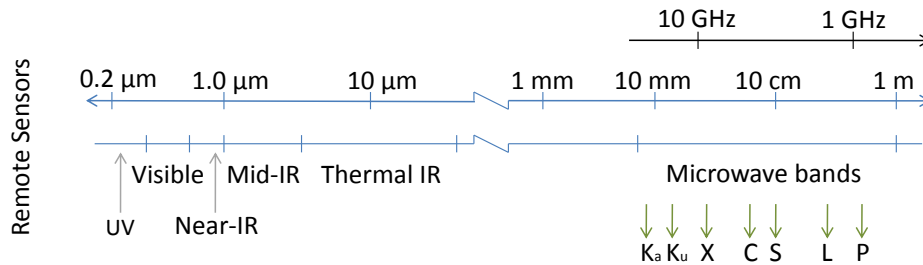
### 3.1 Remote sensing

*In situ* measurements at proper spatial and temporal scales are difficult to obtain in terms of mesoscale to sub-mesoscale processes. When it comes to monitoring marine coastal environments, remote sensing is a highly valuable tool, mainly because of the wide range of scales involved (Johannessen *et al.*, 1996). Satellite remote sensing can be investigated for different phenomenon that may lead to new insight and understanding of the processes that control them, and to a certain degree even the ocean circulation as a whole. This chapter is mainly based on the remote sensing theory found in Robinson (2004), with elements from the article by McCandless & Jackson (2004).

Remote sensing uses different wavelengths of the electromagnetic (EM) spectrum (see Figure 3.1), ranging from the visible light, radio and infrared (IR) wavelengths to the microwaves. Because the area of interest is located in a region that is dark half the year and frequently cloudy, microwave observations are perfect since the EM waves can pass through the clouds and are not dependent on light. It can thus be regarded as an all weather system.

When the wavelength increases from the visible and IR area in Figure 3.1 to the microwave area, the resolution will decrease. However, one instrument using microwaves is capable of outperforming the resolution of IR and visible light; it is the imaging SAR. Its high resolution and large spatial coverage makes SAR a

very powerful tool. SAR images provides information about a number of oceanic features such as surface and internal waves, currents, up-welling, sea ice, fronts, shoals, variable wind velocities, ship traffic, oil spill and even rainfall (Johannessen *et al.*, 1996).



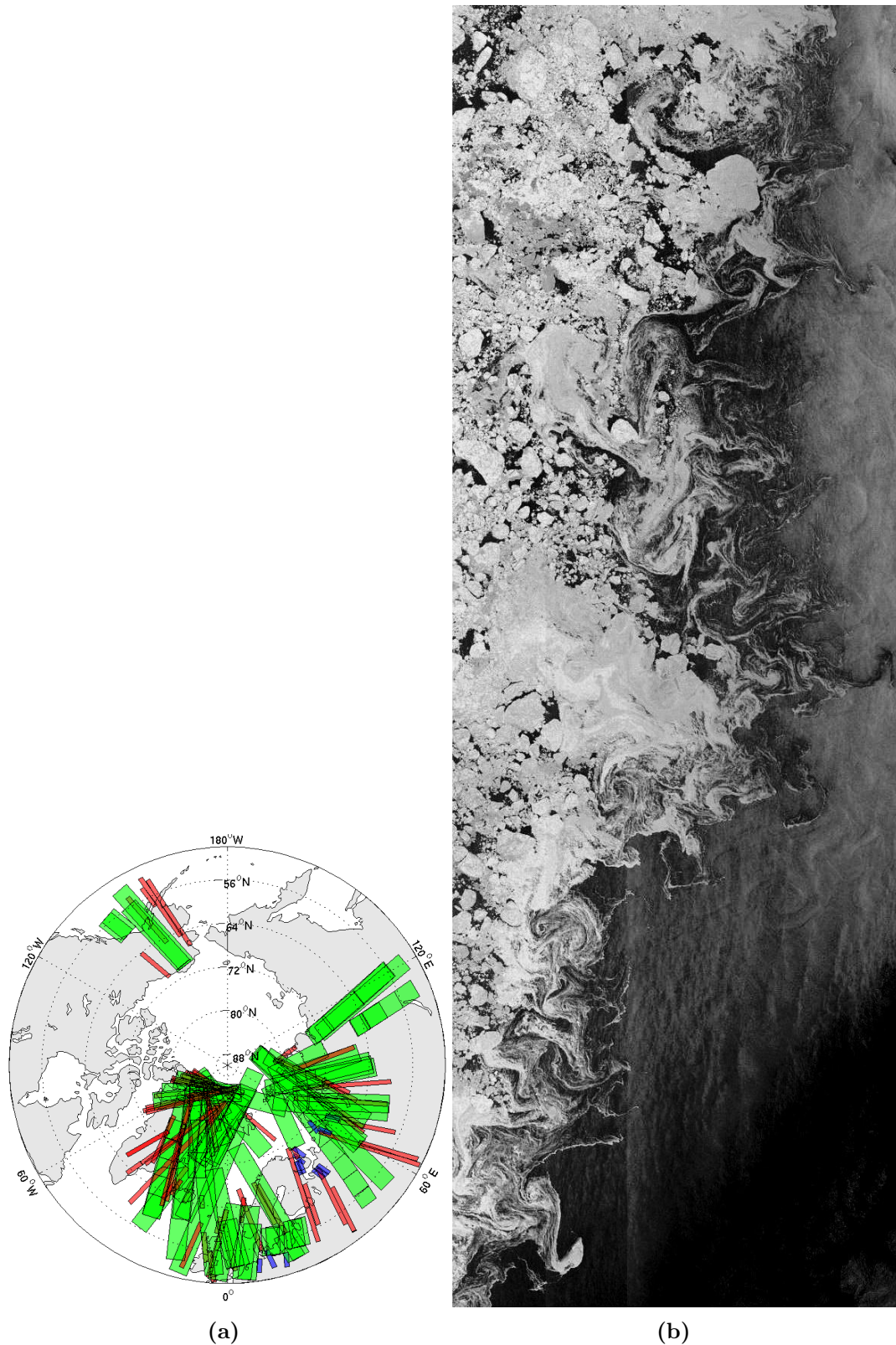
**Figure 3.1:** *The electromagnetic spectrum. Radar and passive radiometers use the wavelengths on the right side. The different names on the microwave bands are also shown. The figure is a modification of the version found in Berens (2011)*

This chapter will cover the principles and methods of data acquisition and interpretation, but before the attention is aimed at the SAR, the instrument providing data for the sea ice extent is briefly presented: The sea ice extent and type data are retrieved from the Advanced Microwave Scanning Radiometer (AMSR-E), situated at the Earth Observing System (EOS) Aqua Satellite. The passive microwave radiometer measures the thermal radiation, also known as the brightness temperature, emitted by the sea surface. It operates on the microwave part of the EM spectrum. More information about the instrument can be found on Spreen & Kaleschke (2011).

### 3.1.1 The Satellite

European Space Agency's (ESA) Environmental Satellite (Envisat) was launched 1st March 2002. It is a sun synchronous polar orbiting satellite, meaning that the satellite passes over the same part of the earth on nearly the same local time. It orbits at an altitude of 790 km ( $\pm 10$  km), has a repeat cycle of 35 days, and a complete coverage of the earth is obtained in 1-3 days. Envisat contains ten instruments that provide measurements of land, ocean, atmosphere and ice. A coverage map for the Envisat ASAR instrument can be seen in Figure 3.2a.

The data from the satellite are transmitted from ESA Satellite station in Kiruna to Nansen Environmental and Remote Sensing Center (NERSC) in Bergen. They are processed and analyzed at NERSC, where an archive with the ASAR images has been made. The archive comprises at the time of writing over 10 000 ASAR images, beginning with July, 2005.



**Figure 3.2:** (a) Map showing the satellite track coverage of ASAR images over the polar area of the northern hemisphere, for nine days in 2005. The green box shows the Wide Swath Mode, the red box the Image Medium Mode and the blue box is the Alternating Polarization Mode. Made by Knut-Frode Dagestad<sup>1</sup>. An example of the WSM can be seen in (b), showing an ASAR image from the 19th May 2009 (descending path, H/H polarized). The size of this image is  $\sim 300 \times 1000$  km.

<sup>1</sup>Researcher, NERSC

### 3.1.2 Advanced SAR (ASAR)

ASAR is an extension of the SAR instruments flown on the European Remote Sensing Satellites (ERS-1 and 2), and is one of the ten instruments operated on Envisat. As the name indicates, it is a more advanced instrument compared to SAR. It uses new technologies with improved performance, like a digital chirp pulse generator, ScanSAR modus, dual polarization and an active group antenna (antenna which both transmits and receives modules).

The ScanSAR technique makes wide area coverage possible. It enables 400 km swath width with a resolution of 150 m or 1 km (Figure 3.2a), depending on the mode. ASAR has seven different swath widths which gives incidence angles ranging from  $15^\circ$  to  $45^\circ$ .

The target classification capability is improved with help from dual polarization. The radar has the possibility to send horizontal or vertical polarized signals, and receive either horizontal or vertical signals, or both. With dual polarization an image is obtained with half of the looks from horizontal polarization, and the second half from vertical polarization.

ASAR can operate in five different modes. Three of them are shown in Figure 3.2a. The green box is the Wide Swath Mode (WSM), which is utilized in this study. The red and blue box are the Image Mode and Alternating Polarization Mode respectively. The two last modes are not included; namely the Global Monitoring Mode and the Wave Mode. An example of an ASAR image obtained from the WSM is shown in Figure 3.2b. Apart from the peculiar properties mentioned above, ASAR and SAR share the same principles.

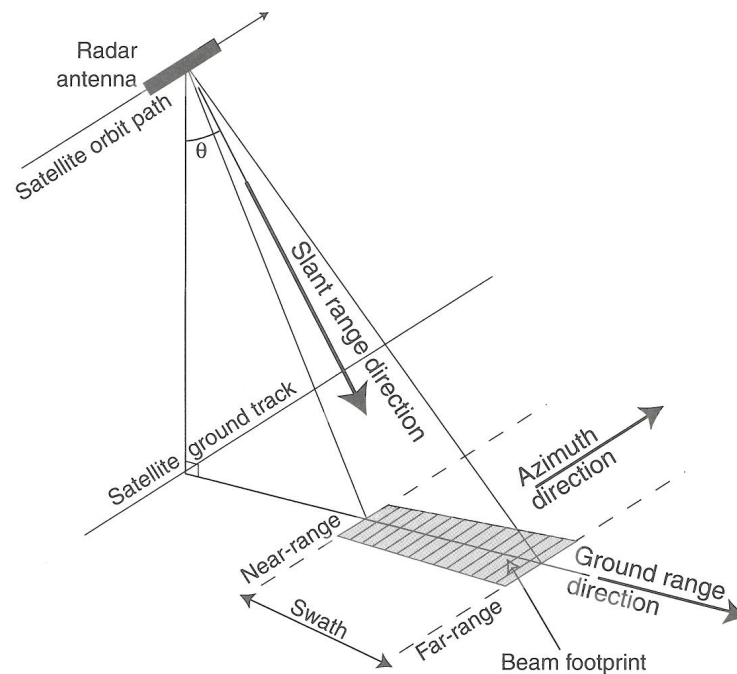
## 3.2 Principles of SAR

In general, the bigger the antenna, the higher resolution, thus enabling more unique information to be reached. The SAR evades this principle. Synthetic aperture means that the radar simulates a huge antenna by utilizing the flight path of the satellite. As the satellite moves, the distance between the antenna and a fixed surface target will vary continually, and the phase for the returned signal will vary in line with the distance. The antenna has an actual length of 10 m, but with the SAR principle it seems as it has an antenna size equal to the distance the SAR-antenna has moved ( $O(10^3)$  m). Without this technique, the



SAR-antenna would have to be 80 times the size of the satellite to achieve the same resolution. For the synthetic aperture principle to work properly, the exact position of the satellite when sending and receiving the signals must be known.

The basic arrangement of a SAR can be seen in Figure 3.3. SAR is an active instrument, it sends out a radar beam that it later receives as backscatter. The pulses are emitted, and the echo is recorded coherently. The radar beam is directed orthogonal to the satellites travelling direction, and the object on the ground will be illuminated for an extended period of time, due to the beam width. By demodulation and compression, the echo has the form of series of several thousand measures of amplitude and phase of the backscattered signal, recorded as a function of time.



**Figure 3.3:** Sketch illustrating the basic arrangement of a satellite SAR. One should notice the definition of azimuth and range, the swath, the incidence angle ( $\theta$ ) and beam footprint. The figure is retrieved from Robinson (2004).

### 3.2.1 Resolution in azimuth and range

The SAR sweeps over the ground like a scanning sensor, collecting data in both the along-track (azimuth) and in the cross-track (range) direction. To gain fine resolution in the azimuth direction, the synthetic aperture principle is applied. The resolution is  $D/2$ , where  $D$  is the apparent length of the antenna. To sharpen

the returned signal the Doppler frequency shift is used. The Doppler shift is unique for every azimuth point in the beam footprint (the grey area in Figure 3.3), since the relative velocity between the point and the radar is unique.

The range resolution is defined as  $c\tau/2\sin\theta$ , where  $c$  is the speed of light,  $\tau$  is the pulse duration and  $\theta$  is the incidence angle. A frequency chirp (linearly modulated pulse) is applied in order to achieve a resolution that is not limited by the pulse duration  $\tau$ .

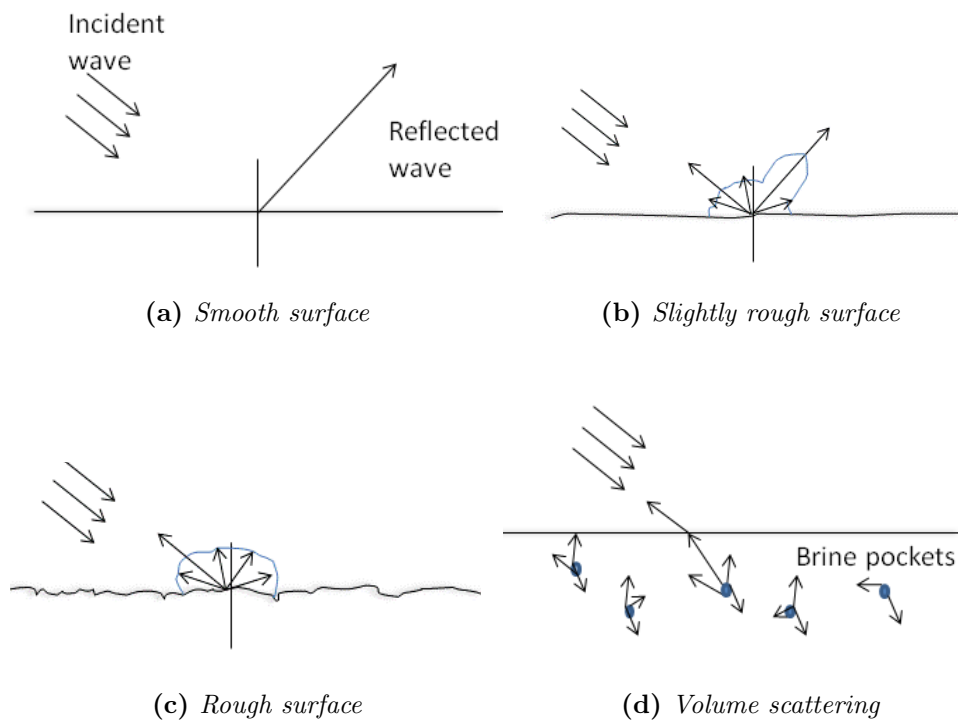
### 3.2.2 Scattering

#### Bragg scattering

The ocean surface experiences a spectrum of waves, from short ripples to waves hundreds of meters long. It is constantly moving with a variety of motions. SAR backscatter is particularly sensitive to the wind induced Bragg waves that have a wavelength of the same order as the EM wavelength projected from the antenna (mm to cm scale). This is called Bragg scattering, a phenomenon known to amplify the backscattered signal.

#### Surface and volume scattering

The signal from the sea ice is backscattered from surface scattering, volume scattering or multiple volume-surface scattering (see Figure 3.4). Surface scattering takes place at the surface. The roughness evident on an image of any scattering surface depends on the radar frequency, polarization and the incidence angle of the beam. The relative importance between these contributions depend on the surface roughness and the dielectric properties of the sea ice. Examples of surface scattering can be seen in Figure 3.4a, 3.4b and 3.4c, which show the backscatter when the surface is smooth, slightly rough or rough, respectively. Volume scattering is scattering within the sea ice, mainly due to the presence of brine pockets. A principle sketch can be seen in Figure 3.4d. The signal from sea ice will vary in a broad range due to variation in ice type, the dielectric properties and spatial distribution of the ice, internal geometry, ice cover, temperature and even the formation conditions.



**Figure 3.4:** Surface scattering in the situation of a smooth surface (a), a slightly rough surface (b), and a rough surface (c). Volume scattering is sketched in (d). The figures are based on a figure in (Robinson, 2004, Figure 9.8).

### 3.3 SAR image interpretation

SAR provides a two dimensional image of the surface, as the example in Figure 3.2b. Each pixel represents an estimation of the backscatter for a confined area on the surface. The dark areas represent low backscatter, while brighter areas can be interpreted as high backscatter. High backscatter means that a large fraction of the energy from the transmitted pulse are returned to the antenna, while low backscatter indicates the opposite. When looking at a radar image, a useful rule-of-thumb is that the brighter area, the rougher the surface.

The magnitude of the backscatter is normally denoted as  $\sigma_0$  and is as mentioned a measure of the surface roughness. The surface roughness is, in addition to wind, influenced by waves, currents, surface films (natural or e.g. oil) and sea ice. The wind generates the sea surface roughness field, and the feature of an ocean phenomenon appears on the image because the phenomenon modulates this wind generated roughness field. With too high wind speed ( $>12 \text{ m s}^{-1}$ ), this modulation is indistinguishable. In contrast, with too calm conditions ( $\leq 2 \text{ m s}^{-1}$ ) the backscatter is close to the SAR noise floor. Small regions of low backscatter

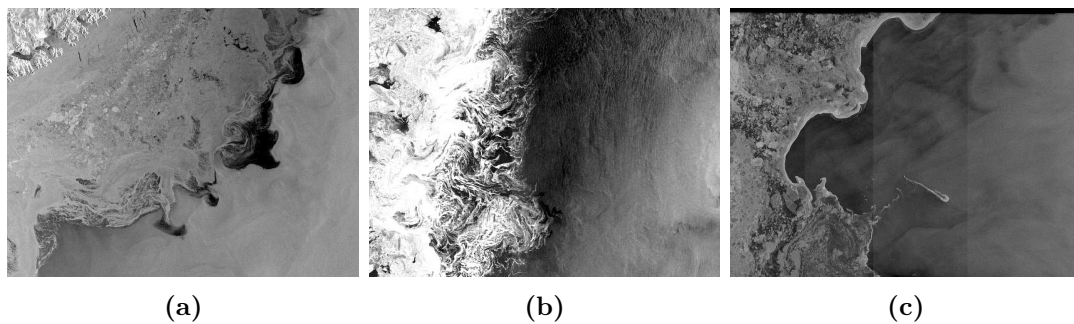
can be found in the SAR images that may be related to damping materials on the surface. These materials may be shed off in case of strong wind. The optimal wind conditions for the SAR are a wind speed between 4 and 12 m s<sup>-1</sup>.

### 3.3.1 Eddy signature

The resolution of the instrument makes it capable of imaging eddies on a broad range of length scales, from 5 to 200 km. The ocean circulation, like the spiraling eddies, can be detected easy if surface manifestations are present. The sea ice act as Lagrangian drifters moving with the current (Shuchman *et al.*, 1987), simplifying the search of eddies. By the presence of these surface manifestations, one can retrieve interesting information about the eddies; their rotational direction, horizontal dimensions, area of sea ice, spiraling structure and with that the eddy asymmetry (Ivanov & Ginzburg, 2002).

During this study, close to 4000 ASAR images have been investigated for the presence of eddies. The eddy characteristics in focus were the size, the area of its presence and the rotational direction. The daily number of eddies and the number of images with eddy signature were also counted.

The interpreting accomplished is a fairly subjective method; two examinations of the same image might differ in the result due to the potential ambiguity. In Figure 3.5, three examples of extracted ASAR images are presented; a clear and indubitable eddy signature can be seen in Figure 3.5a, and a case of doubt in 3.5b. A debatable example is shown in Figure 3.5c; two eddy signatures are evident at the ice boundary even though the sea ice in the eddy is absent. In this thesis, the third example are considered as two adequate eddies. It should be mentioned that it is highly possible that an eddy has been counted several times, a fact that must be taken into consideration when using the data. One can with relative well certainty assume that each eddy is counted twice.



**Figure 3.5:** *Three examples of images with different difficulty regarding interpretation. In the first example, (a), it is easy to manifest at least one eddy. The second, (b), can be ambiguous. (c) has the signature of two eddies at the boundary. The horizontal scale of the images is  $\sim 100$  km.*

### 3.4 Wind retrieval

Information about the wind speed and direction can be obtained from SAR images due to their dependency on the surface roughness,  $\sigma_0$ , relative to the radar viewing direction.  $\sigma_0 = \sigma_0(U, \chi, \theta, p)$ , where  $U$  is the wind speed,  $\chi$  is the direction,  $\theta$  is the incidence angle, and  $p$  is the polarization.  $p$  is a known parameter and  $\theta$  is dependent on the range location. This information reveals the possible combinations of  $U$  and  $\chi$ . One has to know the wind direction so that  $U$  can be solved directly. The CMOD-4 algorithm can be applied to calculate the wind speed (Stoffelen & Anderson, 1997).

The wind direction is estimated from numerical weather prediction models, like HIRLAM or NCEP. HIRLAM, or the High Resolution Limited Area Model, is a European cooperative program that develops a numerical weather prediction system. More details about the HIRLAM can be found in e.g. (HIRLAM, 2010; Uden *et al.*, 2002). The National Centers for Environmental Predictions (NCEP) delivers, among other products, global weather forecasts. More information about this model can be found on (NOAA, 2011).

CMOD-4 provides information about  $\sigma_0$  as a function of relative wind direction, wind speed and incidence angle. The function is given as

$$\sigma_0 = B_0[1 + B_1 \cos \chi + B_2 \cos 2\chi] \quad (3.1)$$

where

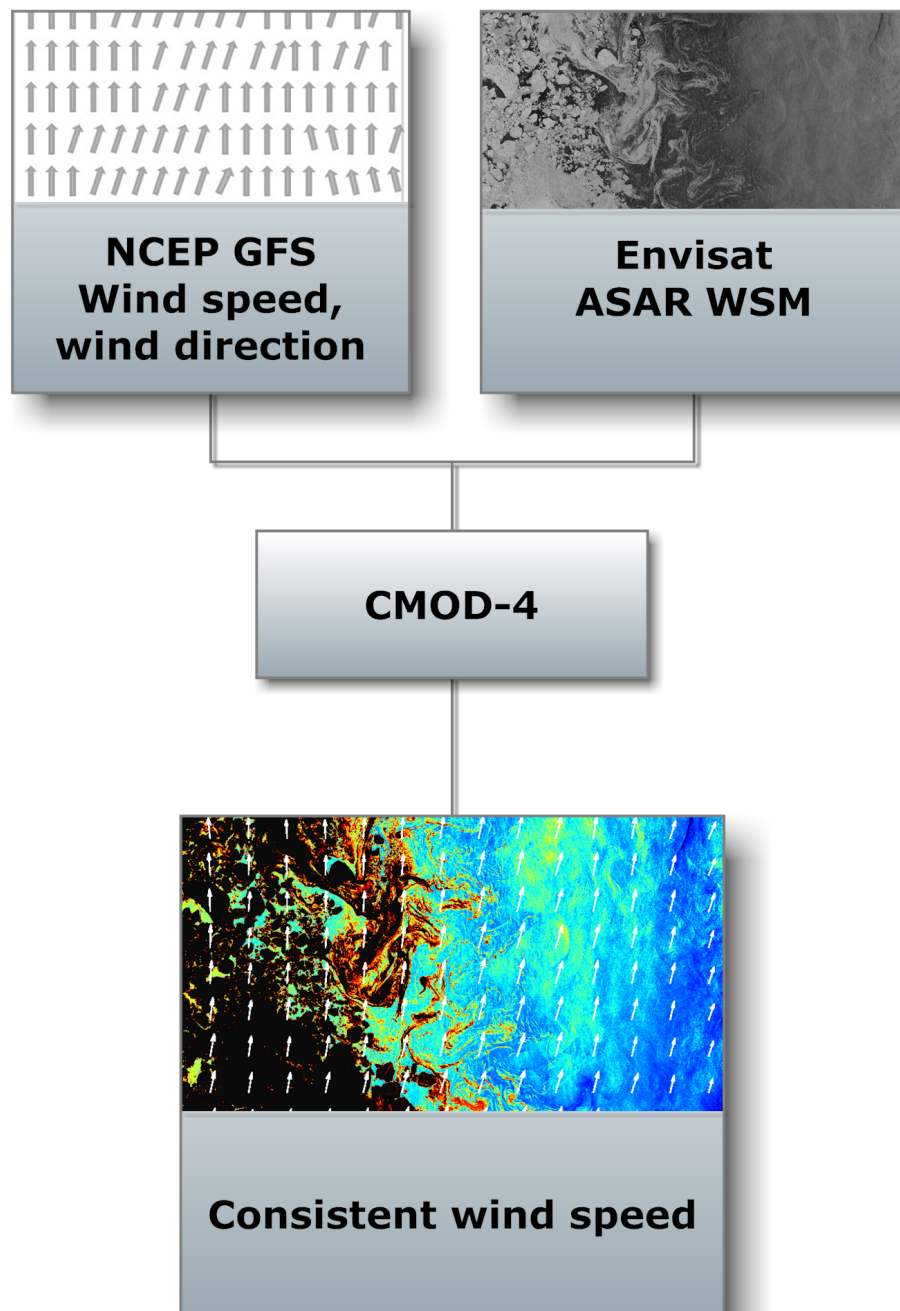
$$B_0 = 10^{\alpha + LUT(\theta) + \gamma f_1(U + \beta)} \quad (3.2)$$

The coefficients in Equation 3.1,  $B_0$ ,  $B_1$  and  $B_2$ , depend on the incidence angle of the radar beam, in addition to the wind speed.  $B_1$  is the upwind/downwind term and  $B_2$  is the upwind/cross-wind term. In Equation 3.2,  $\alpha$  and  $\gamma$  are parabolic functions of  $\theta$  (Stoffelen & Anderson, 1997). The problem with wind speed at the low velocity scale is solved by the parameter  $\beta$ , which has a parabolic dependency on  $\theta$ .  $LUT(\theta)$  must be computed from a comparison between the satellite measured  $\sigma^0$  and European Centre for Medium-Range Weather Forecasts (ECMWF) simulated  $\sigma^0$ .  $f_1(U + \beta)$  depends on the size of  $(U + \beta)$ :

$$f_1(U + \beta) = \begin{cases} -10 & \text{if } (U + \beta) \leq 10^{-10} \\ \log(U + \beta) & \text{if } 10^{-10} < (U + \beta) \leq 5 \\ \frac{\sqrt{(U + \beta)}}{3.2} & \text{if } (U + \beta) > 5 \end{cases} \quad (3.3)$$

The forecast model used in the CMOD-4 algorithm is the NCEP Global Forecast System (GFS) model. The flow chart in Figure 3.6 shows how consistent wind speed data are retrieved by the use of the ASAR data, the NCEP data and the CMOD-4 algorithm.

The estimated wind direction and the solved wind velocity are made available in the same archive as the ASAR images (described in Section 3.1.1). An example of an ASAR image with the appurtenant wind data can be seen in Figure 3.6. Wind data were gathered simultaneously with the eddy data; when an eddy was observed in an image, the wind field data of the same area were collected. In case of two eddies in the same image, the representative mean wind was selected. The weather prediction model used for wind direction is mainly HIRLAM. When HIRLAM does not deliver the data, the NCEP wind direction is invoked. HIRLAM has a poor coverage in Area 3, so NCEP is used as required.



**Figure 3.6:** Flow chart showing the arrangement of CMOD-4 together with wind- and ASAR data. The result, the consistent wind speed, shows the speed (from light blue (weak wind) to black (strong wind)) the direction and the surface signature of the sea ice.





# CHAPTER 4

---

## Results

---

### 4.1 Statistics of eddy occurrence

The occurrence of eddies in the MIZ varies from year to year, month to month and day to day. The total number of eddies in 2008 and 2009 can be found in Table 4.1, it shows that the number of eddies in 2009 exceeds 2008 with 238. Due to the lack of longer time series the variation on a shorter time scale will be in focus from here on.

**Table 4.1:** *The total number of eddies in each month in 2008 and 2009. The total number of each year is given in the last column.*

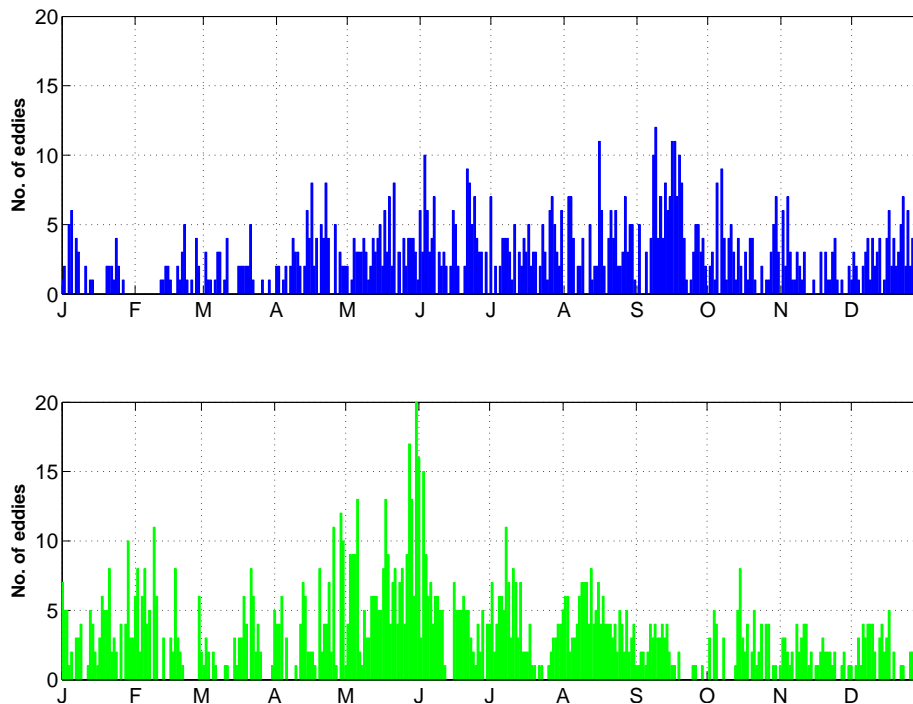
	J	F	M	A	M	J	J	A	S	O	N	D	Total
2008	39	26	35	80	92	108	97	101	145	82	49	95	<b>949</b>
2009	101	84	56	108	225	142	111	140	48	62	52	58	<b>1187</b>

#### 4.1.1 Monthly variability

##### Eddy occurrences

The total number of eddies each month is the intentional subject of Table 4.1. This, in combination with Figure 4.1, highlights the monthly and seasonal vari-

ability of the eddy occurrence. The upper part of Figure 4.1 represent the data from 2008, the 2009 data are in the lower.



**Figure 4.1:** *The annual variation of the occurrence of eddies. The upper has data from 2008 (blue), the lower from 2009 (green).*

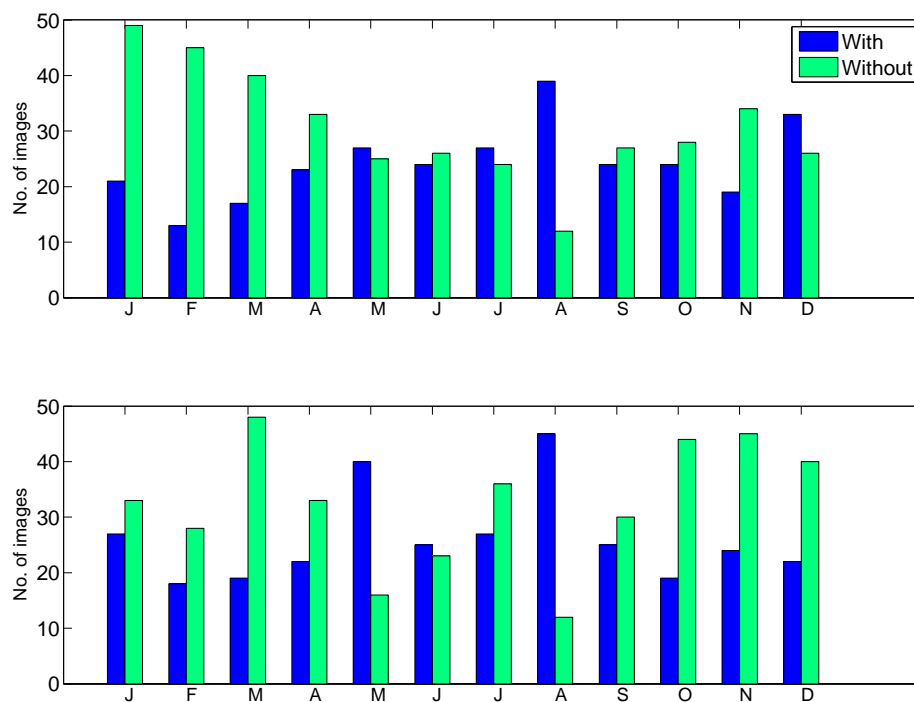
The data from 2008 reveal some eddy activity in the beginning of the year before a draught is apparent in the end of January to mid-February. A rising trend from the last part of February to the beginning of July can be seen, with a maximum in the end of May and in June. July experiences a relatively even distribution of the occurrence of eddies. Another maximum of eddy occurrence is reached in mid-September, with a maximum of twelve in one day. The presence of eddies decrease towards the end of the year, with a slight increase in the end of October and beginning of November, and in December. The month with highest number of eddy occurrences in 2008 is September, the lowest is February (*cf.* 4.1).

The data from 2009 reveal relatively high eddy occurrence in the beginning of the year, compared to 2008. Somewhat more calm conditions are evident in the beginning of March. Then an increase follows toward the end of May, reaching a maximum of twenty eddies per day. Another peak is seen at the beginning of July, but this does not reach the same magnitude. Late summer and early fall experiences some eddy activity, with a decrease towards the beginning of October. Mid-October points out one day with eight eddies present, the rest of the year

shows no intense eddy occurrence. The month with the highest number of eddy occurrences is May, the lowest is September.

Even though the variation is versatile, a common pattern in the two figures can be found: The eddy occurrence is more frequent from the late spring to the early fall, and less frequent rest of the year. With that said, it is worth mentioning that some exceptions exist, e.g. December, 2008 and January, 2009.

The bar charts in Figure 4.2 show the total number of SAR images that contain eddy signature compared to images without the characteristic signature. It does state a similar trend as Figure 4.1.



**Figure 4.2:** The annual variation of eddy images with (blue bars) and without (green bars) eddy signature. The upper has data from 2008, the lower from 2009.

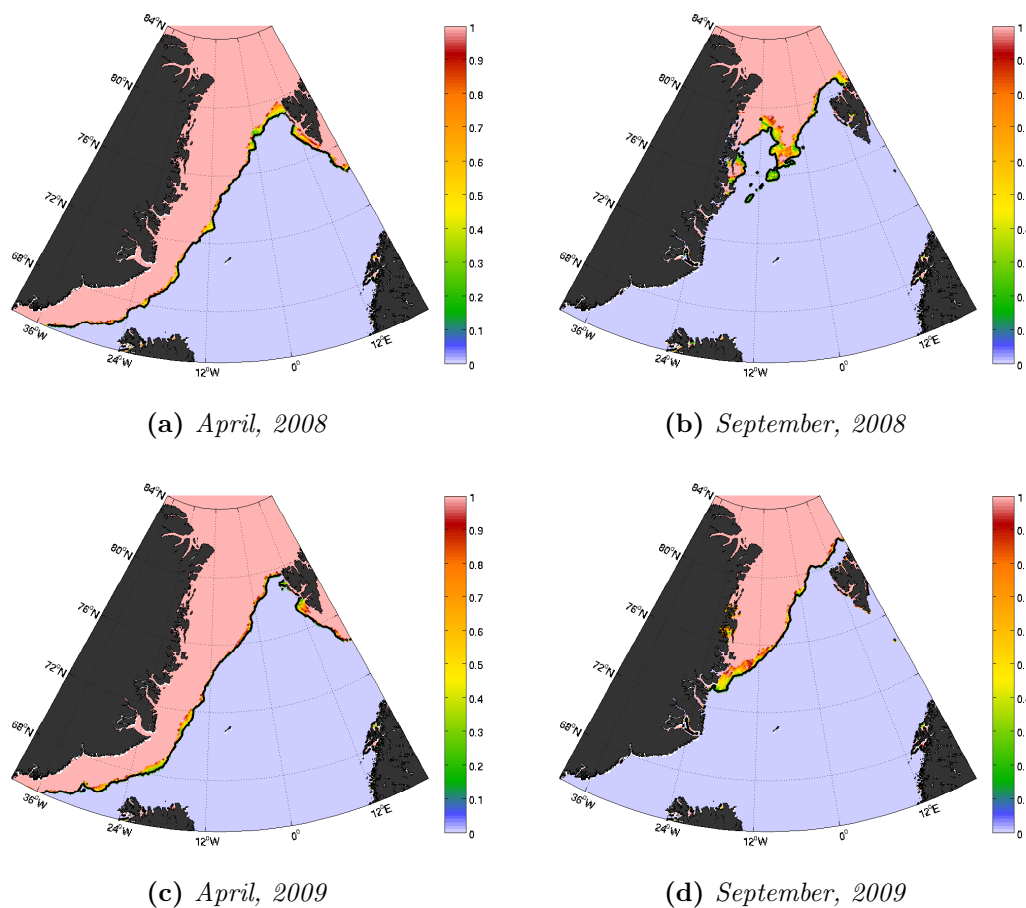
The data from 2008 (upper part) show that there are fewer images with eddies in the beginning of the year, but the number increases relatively steady toward the summer months, followed by a slight decrease the rest of the year. The columns showing images without eddies state the opposite, with many images without eddy signatures in the beginning of the year, a decrease towards the summer and early fall, and again a rise towards the end of the year. Two months does not follow the expected trend; June has less images with eddies than without, December has the opposite.

The data from 2009 (lower part) show in general the same trend. During the

summer months, there exist more images with eddies than without, and oppositely the rest of the year. One exception that is worth mentioning is July, which has less images with than without.

### Sea ice extent

The sea ice extent and composition varies seasonally and annually, in Figure 4.3 one can see the maximum and minimum extent. Maximum occurs normally in the late March and April (Figure 4.3a and 4.3c), and minimum in September (Figure 4.3b and 4.3d). The fraction of the ice cover is indicated with different colours, defined by the colour bar on the right.



**Figure 4.3:** Maximum (left) and minimum sea ice extent in the area of interest. The maximum occurs in the beginning of April, the minimum extent around September. The colour bar to the right represents the fraction of the ice cover (1 = 100%, 0 = ice free surface). The figures are made by Francois Counillon<sup>1</sup> with data from AMSR.

<sup>1</sup>Post-doc, NERSC

The results from the study of the monthly variability (e.g. Figure 4.1) shows that the climax of eddy occurrence is reached around September. Contemplating Figure 4.3 with this in mind, it is evident that the maximum occurs when the sea ice extent is near its minimum.

### 4.1.2 Regional variability

Table 4.2 shows the distribution of eddies by comparing the three areas against each other. Area 1 has almost 39% of the eddy occurrence, Area 2 has 54%, compared to Area 3, which has only approximately 7% (in total for both years).

**Table 4.2:** *The total number of eddies in the three areas with an emphasis on the regional variability. The total number of eddy occurrence highlights the differences. Data from both 2008 and 2009 are included.*

	Area 1	Area 2	Area 3
No. of cyclones	651	881	118
No. of anticyclones	171	276	39
Total	822	1157	157
% cyclones	79	76	75

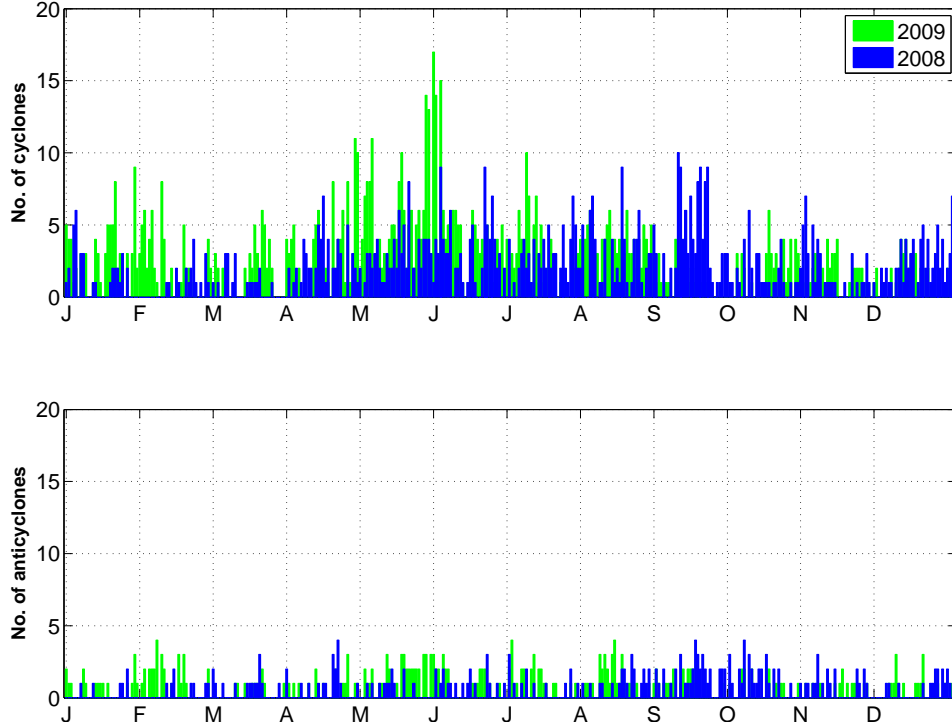
In addition to the regional difference in eddy occurrence, Table 4.2 highlights the relation between cyclonic and anticyclonic rotation in the three areas; Area 1 has 79% cyclones, Area 2 has 76%, while Area 3 has 75%. This difference between cyclones and anticyclones is also the subject of Table 4.3. The number of cyclonic eddies are 734 for 2008 and 916 for 2009, while the total number of anticyclones are 215 in 2008 and 271 in 2009. Some percentage calculations are performed to emphasize the differences;  $\sim 77\%$  of the eddies rotate cyclonic, thus 23% rotate in the opposite direction. This relation applies to both 2008 and 2009.

**Table 4.3:** *The total number of cyclones versus anticyclones. The percentage calculation emphasizes the distinct difference.*

	2008	2009	Total
No. of cyclones	734	916	1650
No. of anticyclones	215	271	486
% cyclones	77	77	77

In search of some possible annual variation of the rotational direction, the yearly distribution of cyclones and anticyclones are investigated (see Figure 4.4). In gen-

eral, the cyclonic distribution (upper part) shows the same pattern as Figure 4.1 and 4.2. The presence of anticyclones (lower part) are relatively even distributed over the two year period, with a maximum of four eddies in the same day.



**Figure 4.4:** Annual variation of the presence of cyclonic (top) and anticyclonic eddies during 2008 (blue) and 2009 (green).

## 4.2 Size

The Rossby radius of deformation is presented in Equation 2.2. To calculate the radius one must have *in situ* data covering the area. This can be found by inspecting the hydrographic sections in the paper by (Johannessen *et al.*, 1987a, Their figure 4(c,d)). The sections are taken during MIZEX'84 in the area between 78-79° N, but are assumed applicable for the entire area. The calculation of the Rossby radius and the dimensionless Rossby number in the three areas are given in Table 4.4.

The Rossby number is of  $O(10^{-2})$ . By definition, the eddies will thus be referred to as quasi-geostrophic. The mean radius of the eddies are set to 30 km ( $\pm 5$  km). In comparison, the deformation radius is approximately 4 km in the MIZ. That means that the eddies will run their course in accordance with geostrophic balance.

**Table 4.4:** Overview of the important values regarding eddy characteristics.  $\theta$  is the latitude,  $f$  is the Coriolis parameter and  $\beta$  is the variation of Coriolis with latitude. These are parameters used in the calculation of the Rossby number ( $R_0$ ) and the Rossby radius of deformation ( $R_d$ ).

	$\theta$ [° N]	$f$ [s <sup>-1</sup> ]	$\beta$ [s <sup>-1</sup> ]	$R_d$ [km]	$R_o$
Area 1	79	$1.43 * 10^{-4}$	$2.78 * 10^{-5}$	<b>3,75</b>	<b>0,0160</b>
Area 2	74	$1.40 * 10^{-4}$	$4.02 * 10^{-5}$	<b>3,83</b>	<b>0,0163</b>
Area 3	67	$1.34 * 10^{-4}$	$5.70 * 10^{-5}$	<b>4,00</b>	<b>0,0178</b>

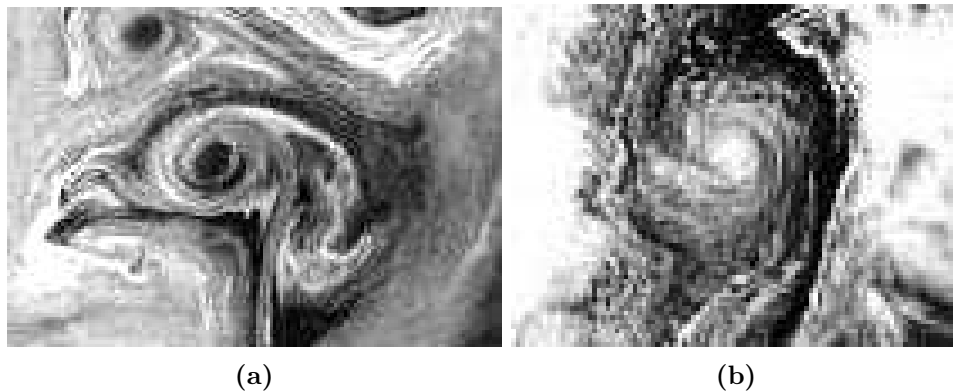
The Rossby radius of deformation varies with both region and season. The regional variation is due to the Coriolis parameters ( $f$ ) dependency on latitude; the deformation radius decreases with the distance from the Equator, as seen in Table 4.4.

The deformation radius depends on both the density difference and the depth of the mixed layer. These are parameters that varies with the season. In the winter  $H$  is thicker the density difference is lower than in the summer. During winter, the radius is closer to the  $O(10^1)$  (Häkkinen, 1986).

### 4.2.1 The amount of sea ice trapped in the eddy

The eddies move sea ice away from the ice edge and into the warmer water. This amount of removed sea ice is interesting to quantify. The amount depends on the area of the eddy. An eddy is capable of trapping  $(\pi r^2)/2$  km<sup>2</sup> of sea ice, when assuming that 50% of the eddy is covered with ice. This equals 1413.7 km<sup>2</sup>, using a mean radius of 30 km. The thickness of the ice is not possible to directly estimate from the satellite sensor used, so a representative thickness is invoked. Assuming an ice thickness of 1.5 m the volume of sea ice in an eddy is calculated to be 2 km<sup>3</sup>.

The anticyclones have an advantage of trapping the ice in the centre over cyclonic eddies, as described in Section 2.5.2. Two contradictory examples found in the MIZ can be seen in Figure 4.5 and in Figure 4.6. In both figures, (a) shows little sea ice in the centre, whereas (b) shows a more gathering case.



**Figure 4.5:** An example showing the difference of the amount of sea ice in two cyclonic eddies. The eddy in (a) contain less sea ice than the one in (b). The diameter of (a) is around 25 km, while (b) is close to 40 km.



**Figure 4.6:** An example showing the difference of the amount of sea ice in two anticyclonic eddies. The eddy in (a) contain less sea ice than the eddy in (b). The diameter of (a) is around 60 km, while (b) has a diameter of approximately 50 km.

### 4.3 Wind influence

Table 4.5 and 4.6 show the number of eddies traceable during different wind direction and intervals. The tables are a reproduction of data found in Appendix B, but with a more straightforward presentation of the wind. The data from Area 1, Area 2 and Area 3 are represented in separate sub-tables. It should be noted that eddies without wind data are excluded from these tables. The wind velocity is given in four intervals, the same intervals as the wind rose is separated into. The circles of the wind rose denote the percentage of one particular wind direction.



**Table 4.5:** The three sub-tables show the total number of eddies for each month of 2008. (a) covers Area 1, (b) Area 2 and (c) covers Area 3. Wind direction and velocity [ $m s^{-1}$ ] are given in four intervals; Blue=[0-6], Green=[7-11], Yellow=[12-15] and Red= $>15$ . The wind rose can be interpreted as a histogram; the circles represent the percentage of the wind with that particular direction where the outermost circle is 15% and the inner is 5%.

(a) Area 1

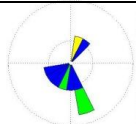
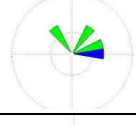
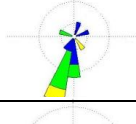
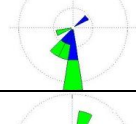
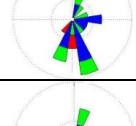
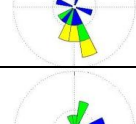
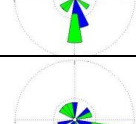
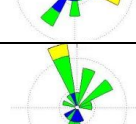
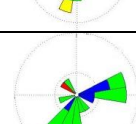
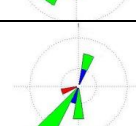
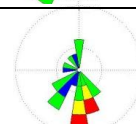

Month	Total	Wind Velocity	Wind Direction
January	6	[0-6]	
	2	[7-11]	
	1	[12-15]	
	0	>15	
February	1	[0-6]	
	3	[7-11]	
	0	[12-15]	
	0	>15	
March	6	[0-6]	
	5	[7-11]	
	2	[12-15]	
	0	>15	
April	6	[0-6]	
	5	[7-11]	
	0	[12-15]	
	0	>15	
May	10	[0-6]	
	8	[7-11]	
	0	[12-15]	
	2	>15	
June	6	[0-6]	
	4	[7-11]	
	3	[12-15]	
	0	>15	
July	5	[0-6]	
	9	[7-11]	
	0	[12-15]	
	0	>15	
August	9	[0-6]	
	8	[7-11]	
	1	[12-15]	
	0	>15	
September	6	[0-6]	
	17	[7-11]	
	2	[12-15]	
	0	>15	
October	6	[0-6]	
	12	[7-11]	
	0	[12-15]	
	1	>15	
November	2	[0-6]	
	7	[7-11]	
	0	[12-15]	
	1	>15	
December	5	[0-6]	
	2	[7-11]	
	2	[12-15]	
	2	>15	

Table 4.5: *Continued*(b) *Area 2*

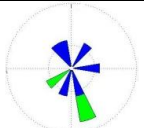
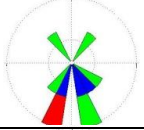
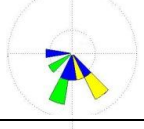
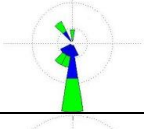
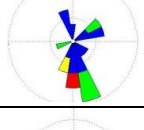
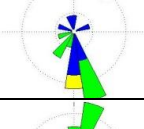
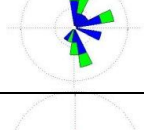
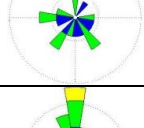
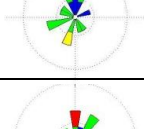
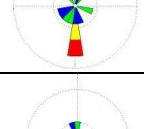
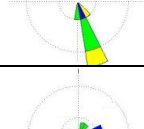
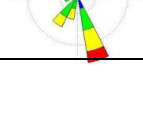
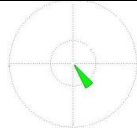
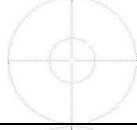
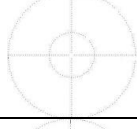
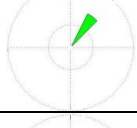
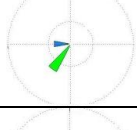
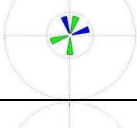
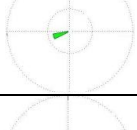
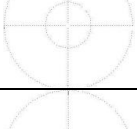
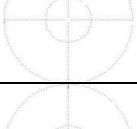
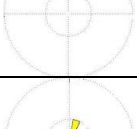
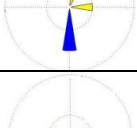
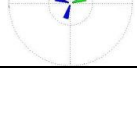
Month	Total	Wind Velocity	Wind Direction
January	6	[0-6]	
	2	[7-11]	
	0	[12-15]	
	0	>15	
February	3	[0-6]	
	5	[7-11]	
	0	[12-15]	
	1	>15	
March	4	[0-6]	
	2	[7-11]	
	2	[12-15]	
	0	>15	
April	8	[0-6]	
	7	[7-11]	
	0	[12-15]	
	0	>15	
May	13	[0-6]	
	4	[7-11]	
	1	[12-15]	
	1	>15	
June	9	[0-6]	
	7	[7-11]	
	1	[12-15]	
	0	>15	
July	13	[0-6]	
	9	[7-11]	
	0	[12-15]	
	0	>15	
August	8	[0-6]	
	8	[7-11]	
	0	[12-15]	
	0	>15	
September	5	[0-6]	
	12	[7-11]	
	2	[12-15]	
	0	>15	
October	6	[0-6]	
	6	[7-11]	
	1	[12-15]	
	2	>15	
November	2	[0-6]	
	5	[7-11]	
	2	[12-15]	
	0	>15	
December	3	[0-6]	
	10	[7-11]	
	3	[12-15]	
	1	>15	

Table 4.5: *Continued*(c) *Area 3*

Month	Total	Wind Velocity	Wind Direction
January	0	[0-6]	
	1	[7-11]	
	0	[11-15]	
	0	>15	
February	0	[0-6]	
	0	[7-11]	
	0	[11-15]	
	0	>15	
March	0	[0-6]	
	0	[7-11]	
	0	[11-15]	
	0	>15	
April	0	[0-6]	
	1	[7-11]	
	0	[11-15]	
	0	>15	
May	1	[0-6]	
	2	[7-11]	
	0	[11-15]	
	0	>15	
June	2	[0-6]	
	3	[7-11]	
	0	[11-15]	
	0	>15	
July	0	[0-6]	
	1	[7-11]	
	0	[11-15]	
	0	>15	
August	0	[0-6]	
	0	[7-11]	
	0	[11-15]	
	0	>15	
September	0	[0-6]	
	0	[7-11]	
	0	[11-15]	
	0	>15	
October	0	[0-6]	
	0	[7-11]	
	0	[11-15]	
	0	>15	
November	2	[0-6]	
	0	[7-11]	
	2	[11-15]	
	0	>15	
December	3	[0-6]	
	1	[7-11]	
	0	[11-15]	
	0	>15	

**Table 4.6:** The three sub-tables show the total number of eddies for each month of 2009. (a) covers Area 1, (b) Area 2 and (c) covers Area 3. Wind direction and velocity [ $m s^{-1}$ ] are given in four intervals; Blue=[0-6], Green=[7-11], Yellow=[12-15] and Red= $>15$ . The wind rose can be interpreted as a histogram; the circles represent the percentage of the wind with that particular direction, where the outermost circle is 15% and the inner is 5%.

(a) Area 1

Month	Total	Wind Velocity	Wind Direction
January	6	[0-6]	
	10	[7-11]	
	3	[11-15]	
	0	>15	
February	2	[0-6]	
	5	[7-11]	
	1	[11-15]	
	1	>15	
March	6	[0-6]	
	3	[7-11]	
	2	[11-15]	
	3	>15	
April	5	[0-6]	
	7	[7-11]	
	2	[11-15]	
	2	>15	
May	8	[0-6]	
	11	[7-11]	
	1	[11-15]	
	0	>15	
June	13	[0-6]	
	5	[7-11]	
	0	[11-15]	
	0	>15	
July	15	[0-6]	
	8	[7-11]	
	0	[11-15]	
	0	>15	
August	17	[0-6]	
	8	[7-11]	
	0	[11-15]	
	0	>15	
September	5	[0-6]	
	8	[7-11]	
	0	[11-15]	
	0	>15	
October	4	[0-6]	
	4	[7-11]	
	1	[11-15]	
	1	>15	
November	10	[0-6]	
	9	[7-11]	
	1	[11-15]	
	0	>15	
December	5	[0-6]	
	9	[7-11]	
	1	[11-15]	
	1	>15	

Table 4.6: *Continued*(b) *Area 2*

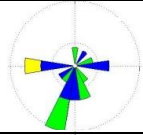
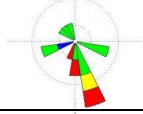
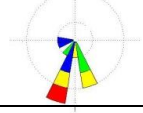
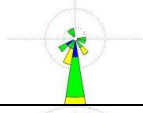
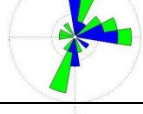
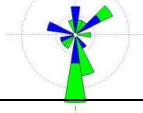
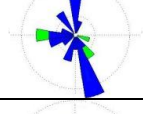
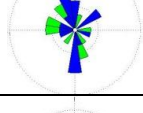
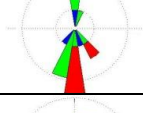
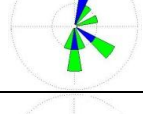
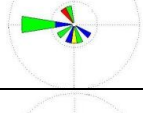
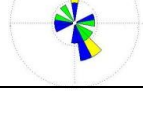

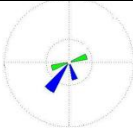
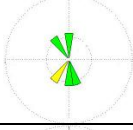
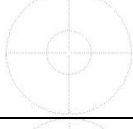
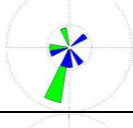
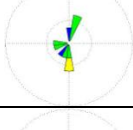
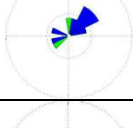
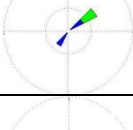
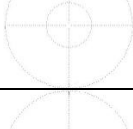
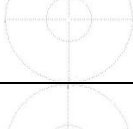
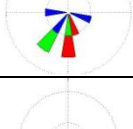
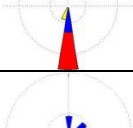
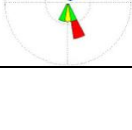
Month	Total	Wind Velocity	Wind Direction
January	10	[0-6]	
	7	[7-11]	
	1	[12-15]	
	0	>15	
February	1	[0-6]	
	9	[7-11]	
	1	[12-15]	
March	3	>15	
	4	[0-6]	
	3	[7-11]	
April	3	[12-15]	
	13	[0-6]	
	4	[7-11]	
May	0	>15	
	14	[0-6]	
	15	[7-11]	
June	0	[12-15]	
	0	>15	
	7	[0-6]	
	10	[7-11]	
July	0	[12-15]	
	0	>15	
	23	[0-6]	
	3	[7-11]	
August	0	[12-15]	
	0	>15	
	17	[0-6]	
	8	[7-11]	
September	3	[0-6]	
	7	[7-11]	
	1	[12-15]	
October	3	>15	
	4	[0-6]	
	6	[7-11]	
November	0	[12-15]	
	0	>15	
	3	[0-6]	
	5	[7-11]	
December	1	[12-15]	
	1	>15	
	8	[0-6]	
December	5	[7-11]	
	2	[12-15]	
	0	>15	

Table 4.6: *Continued*(c) *Area 3*

Month	Total	Wind Velocity	Wind Direction
January	3	[0-6]	
	2	[7-11]	
	0	[12-15]	
	0	>15	
February	0	[0-6]	
	4	[7-11]	
	1	[12-15]	
March	0	[0-6]	
	0	[7-11]	
	0	[12-15]	
	0	>15	
April	5	[0-6]	
	4	[7-11]	
	0	[12-15]	
	0	>15	
May	3	[0-6]	
	6	[7-11]	
	1	[12-15]	
	0	>15	
June	6	[0-6]	
	3	[7-11]	
	0	[12-15]	
	0	>15	
July	2	[0-6]	
	1	[7-11]	
	0	[12-15]	
	0	>15	
August	0	[0-6]	
	0	[7-11]	
	0	[12-15]	
	0	>15	
September	0	[0-6]	
	0	[7-11]	
	0	[12-15]	
	0	>15	
October	3	[0-6]	
	2	[7-11]	
	0	[12-15]	
	2	>15	
November	2	[0-6]	
	0	[7-11]	
	1	[12-15]	
December	3	>15	
	2	[0-6]	
	2	[7-11]	
	1	[12-15]	
	1	>15	

Strong winds are here defined to have velocities  $\geq 12 \text{ m s}^{-1}$ , with moderate winds following as  $< 12 \text{ m s}^{-1}$ . With this in mind, one can see from the first table (4.5) that eddies are observed even though the wind is supposed to be too strong. In Area 1, this is the case in every month, except February, April and July. The latter two months also experience calm conditions in Area 2 in addition to January and August. Area 3 experiences relative strong wind from west in November, the conditions are calm beyond that. One common feature regarding eddy occurrence in spite of strong wind is that the wind is mainly directed from the north or the south, with a majority of the wind-from-north case. When it comes to the wind with lower speed, a typical direction can not be manifested. In cases with a high percentage of a particular wind event, the wind is from north of south, again with a higher number with wind from the north. Exceptions exist however, as in Area 1 in October, which contain eddies during a western wind field. A general seasonal cycle can be drawn; the highest wind speeds occur in the beginning and end of the year (the late fall and winter months), with May as an exception. More calm conditions are evident in the summer months (June, July and August).

In 2009 (Table 4.6) the same trend regarding wind with high speed applies; north or south directed wind does not erase the eddy signature. The majority of wind from north still applies. Some exceptions worth mentioning is in March and May in Area 1, where strong winds from east and west, respectively, are evident, and in January in Area 2, showing strong easterly wind. Area 3 experiences strong wind from the north, which is especially strong at the end of the year. When a high number of eddies is evident, the wind is mainly directed from the north, but also situations with a southerly wind are registered. The seasonal cycle regarding the highest wind velocities is more prominent in 2009 than in 2008. From the beginning of the year until April, the highest velocities are experienced, and the same applies from September to December. The summer months show mainly calm conditions.

Most eddies are found in the summer when the wind fields are predominantly weak to moderate. It is noticeable that eddies exist even when both wind direction and wind velocity would indicate a signature free surface.

## 4.4 Retreat of the ice edge

In Section 4.2.1 the area of sea ice in an eddy were found to be  $1413.7 \text{ km}^2$ . The total number of eddies during a year were counted to be around 1000, but are here

assumed to be 500, since the total number must be regarded as an overestimation (due to the likelihood of counting the same eddy several times, as mentioned in Section 3.3.1). By multiplying the number of eddies (500) with the amount of sea ice in an eddy, the yearly effect of the eddies amounts to  $0.7 \times 10^6$  km<sup>2</sup>. By considering the ice edge in Figure 4.3, a yearly mean extent of  $\sim 1000$  km can be assumed. The mean ice loss along the entire edge is thus 700 km each year.

How efficient the sea ice trapped in the eddy melts is considered next. Table 4.7 holds the values used. The thickness of the ice is assumed to be in a range between 0.5-4.0 m. The mean bottom ablation is  $0.38$  m d<sup>-1</sup> (Josberger, 1987). It will thus take 1.3-10.5 days for an eddy to melt the ice it has captured. An eddy that contains sea ice with a mean thickness of 1.5 m will use 4 days to completely melt it all, independent of the horizontal extent of the ice.

**Table 4.7:** *The range of values for the different terms in Equation 2.8 together with the values used in the calculation.*

Variable	Value	Range	Unit
h = Thickness of sea ice	1.5	0.5 - 4.0	m
ice = Percentage of ice in the eddy	50	10 - 50	%
l = Eddy separation distance	100	60 - 200	km
w = Bottom Ablation	0.38	0.25 - 0.50	m d <sup>-1</sup>
r = Radius	30	20 - 40	km

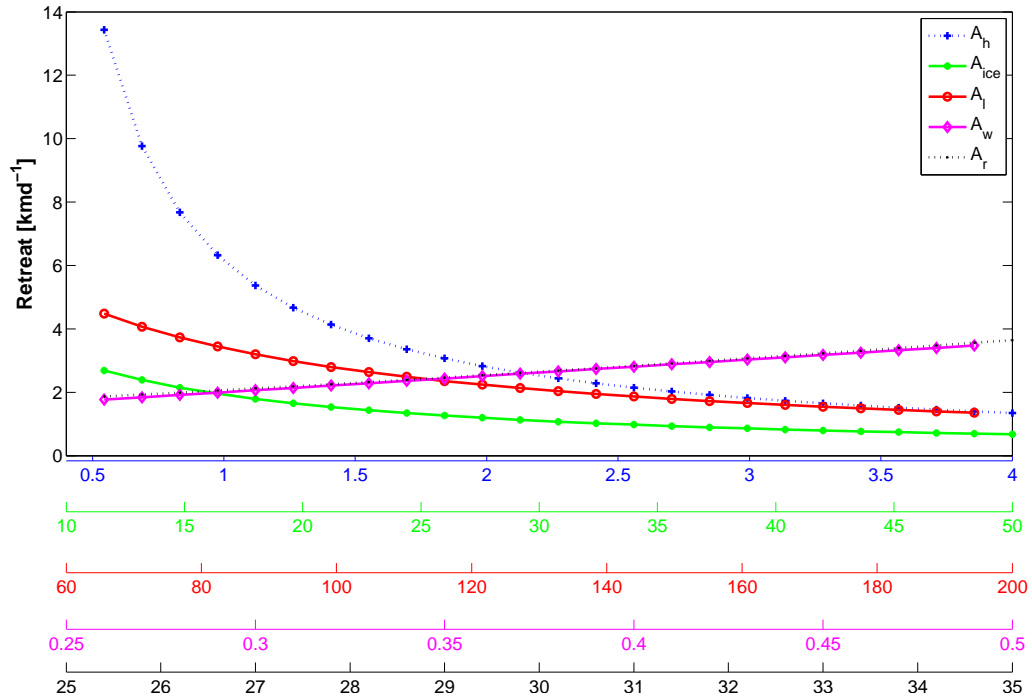
When calculating the daily zonal retreat of the ice edge, the usefulness of Equation 2.8 makes it worth repeated:

$$A = \frac{w\pi r^2}{2lh}$$

It depends on the five parameters listed in Table 4.7. By inserting the values from this table in Equation 2.8 one will get an average retreat of the ice edge of  $3.5$  km d<sup>-1</sup>. This is an average for a length ( $l$ ) of the sea ice (here 100 km). By again using a mean ice extent of 1000 km, the daily retreat of the entire ice edge becomes  $35$  km d<sup>-1</sup>.

The respective impact of the five parameters on the retreat is given in Figure 4.7.





**Figure 4.7:** The retreats dependency on the varying parameters in Equation 2.8, the parameters are plotted against each other to see the contribution from each of them. The subscripts used are  $h$ , the thickness of the ice;  $ice$  denotes the percentage of ice in one eddy;  $l$  is the distance between the center of two neighbouring eddies;  $w$  is the bottom ablation; and  $r$  is the radius.

### The parameters

When the ice is thin, the retreat is high, while the retreat diminishes in relation to the thicker ice. This can be seen from Figure 4.7, presented by the blue line. The thickness of the ice,  $h$ , varies with the season in the range of 0.5-4.0 m. In the summer this range is narrow, with mainly MY to FY ice present. The range is wider in the winter as new ice formation occurs. FY is relatively thin (typically  $O(10^0)$  m). MY ice has survived at least one summer melting season and is thus thicker than the FY ice (typically  $>2.5$  m). It is here assumed an ice thickness of 1.5 m. The ice has had the possibility of growing for a while, but still not to extreme thickness.

The effect of high (50%) or low (10%) ice concentration in an eddy is highlighted by  $ice$  (green line). Low ice concentration contributes to a higher retreat than eddies with higher ice concentration. In summer this is related to the absorption of heat from the solar radiation. The sea ice has high albedo ( $\sim 0.85$ ), so with sea ice present a high proportion of the solar radiation is reflected. Open water

absorbs radiation (albedo  $<0.1$ ). With reduced ice concentration in the eddy, the solar absorption is increased. The melting thus increase when the fraction of sea ice in an eddy decreases. A value of 50% is used in the calculation, a relatively good approximation argued by taking a close examination of the distinct eddy in Figure 3.2b, located right west of Svalbard and a bit south of the Molloy Deep. The frictional forces between the ice floes does also have a contribution, but the exact influence is difficult to state. The amount of sea ice in an eddy is also related to the life cycle of the eddy.

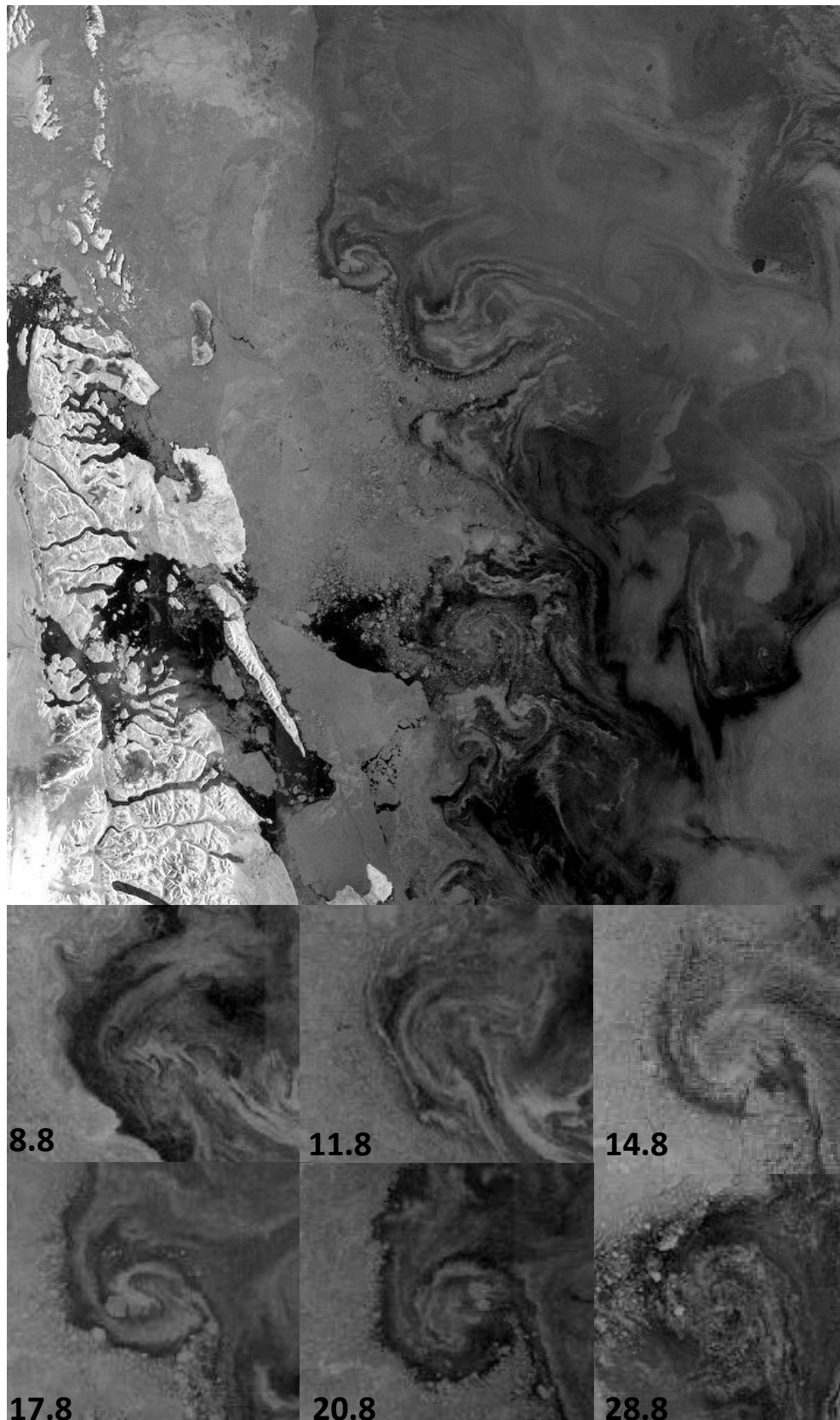
The next parameter is the effect of eddy-eddy interaction. The distance between two neighbouring eddies,  $l$ , contribute to increased retreat when eddies are in close proximity of each other. This indicates that separate eddies have an influence on each other. It should be mentioned that the frequency in the zonal direction is not emphasized. In Figure 4.7,  $l$  is given by the red line. Since the mean radius is 30 km, the minimal value of  $l$  is 60 km ( $2 \times r$ ). The maximum distance is here assumed to be 200 km. The distance of 100 km represent a common scenario, founded by evaluating a number of images, e.g. Figure 3.2b.

The sea ice floes in the MIZ are found to have a diameter of less than 1 km (Gascard *et al.*, 1988), predominantly formed by wave propagation into the MIZ. This is confirmed in the article by Johannessen *et al.* (1987a), where they observe relative small ice floes (200 m across). In Section 2.5.1, the contribution from bottom versus lateral melt was highlighted. The relation between the area of the circumference versus the area of the bottom is calculated to be 1:70 when the ice floe is assumed to have a diameter of 200 m. Thus the bottom ablation has the biggest contribution, a result that is confirmed by Josberger (1987). The bottom ablation,  $\omega$ , is based on his findings. It is highly variable, both in time and space. It depends on the temperature elevation above the freezing point, which again depends on the salinity of the water. A salinity of 32 was assumed as a mean for the whole area. In cases when the relative speed between water and ice increases, the melting is enhanced. Bottom ablation is not the only process that results in ice destruction along the ice edge. Surface waves and ice floe collisions will also have a contribution, in addition to lateral melt. The lateral melt will have an increasing importance as the size of the ice floes decrease. These additional ablation effects are not included in the calculation. The increasing retreat depends linearly on the increasing bottom ablation.

It is found that the retreat of the ice edge increases in step with increasing radius (black line). Eddies with large horizontal extent contributes to a higher retreat

of the ice edge due to the amount of sea ice it can trap and remove. It should be noted that an abundance of small eddies may have a bigger contribution than a few big ones.

In Figure 4.8 six images from different days are presented in a mosaic to see how the sea ice content in an eddy evolve. A cyclonic ice edge eddy with a mean diameter of 30 km started to form around  $77^{\circ}\text{N}$  and  $\sim 18^{\circ}\text{W}$ . Its presence is traceable from 4th August to 10th September. It may be present for even longer time, but this is not verified by the satellite. Based on the amount of sea ice in the eddy centre, the assumed full development of the eddy was reached between 14th and 17th of August.



**Figure 4.8:** *The evolution of an eddy in twenty days. The upper image shows the location of the eddy (approximately  $77^{\circ}$  N and  $18^{\circ}$  W). The six sub-images show an in-zoom of one chosen eddy with a mean diameter of 30 km. The evolution and the beginning of the decay can be seen. The exact date of acquisition is shown in the lower left corner of each sub-image.*

# CHAPTER 5

---

## Discussion

---

### 5.1 Regional and seasonal variation

#### Regional

The occurrence of eddies varies in the three areas of interest; 39% of the eddies are located in Area 1, 54% in Area 2 and only 7% in Area 3.

The most important factor when explaining this regional variability is the uneven division of the three areas. Area 1 has a length of approximately 220 km, Area 2 is much bigger with a length of 880 km, while Area 3 has a length around 500 km where eddies likely occur.

The regional variability is also related to the seasonal variation of the location of the ice edge, *cf.* Figure 4.3. The varying balance between northward and westward advection of near-surface oceanic heat, and the southward and eastward wind-driven ice drift is indicated as determining factors deciding the location of the ice edge (McPhee *et al.*, 1987). There are evidence of sea ice eddies even though the sea ice do not extend all the way south to the area where the eddies are located. This situation are found in Table 4.5 and 4.6, compared with the sea ice extent in Figure 4.3b and 4.3d. A typical example is Area 3 in the summer months. This contradiction may be explained by the resolution of the AMSR data the sea ice extent figures are based on (12.5 km). The interfering from land also impoverish the data; a reduced data quality must be assumed in a band of

50-100 km near land (Johannessen, 2011).

Another factor is the different generation mechanisms, most comprehensible the varying bathymetry in the different areas. For example, the generation mechanism related to the topography is only relevant if the bathymetry contains sea mounts or deeps. Most of the observations of eddies are made in areas where structures like these are not represented (typically Area 2). The eddies that are advected from the WSC tend to follow fracture zones and ridges, as described briefly in Section 2.4. The bathymetric chart in Figure 2.1 gives an immediate explanation why this generation mechanism elevate the occurrence in the northern part of the area.

As mentioned in Section 2.2.1, Johannessen *et al.* (1983) suggested an ice edge jet in the EGC to describe the motion of ice floes they observed. They also observed horizontal current shear between EGC and the recycled AW, and noted that an inflection point existed in the area of the current shear. Thus, the mean kinetic energy can be transferred to the eddies. The vicinity to this jet is thus a factor that may explain the variability.

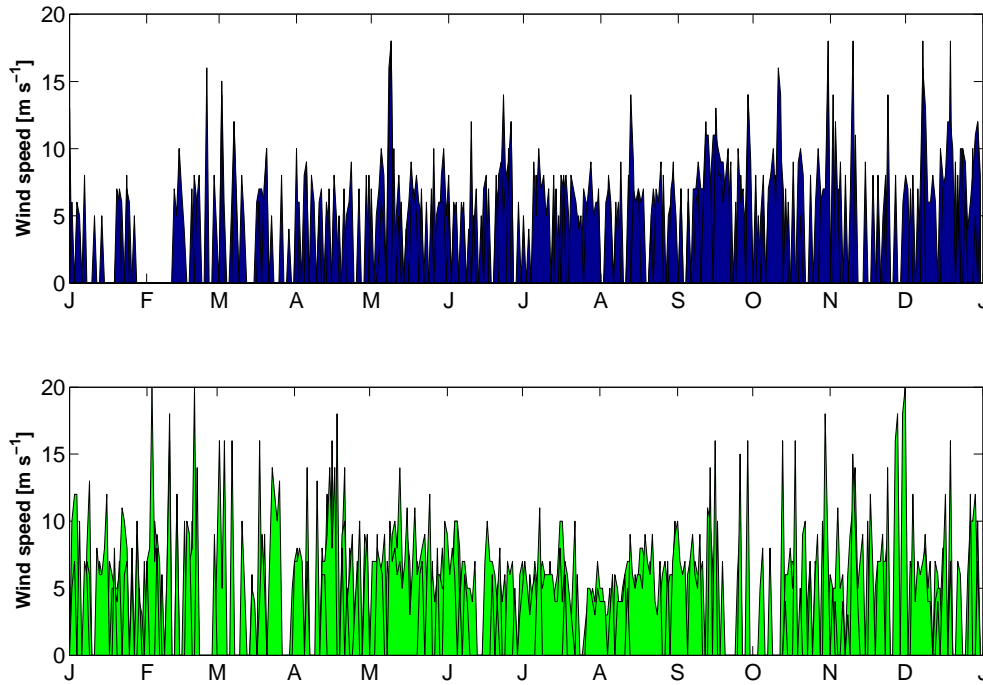
## Seasonal

The seasonal distribution of the occurrence of eddies shows in general the same trend over the two years; the winter and early spring experience less eddies than the late spring, summer and early fall. This applies despite the fact that the extent of the sea ice is much smaller in these months compared to the winter season.

The reason why eddies occur more frequent during the summer months might be due to the wind force. By studying Table 4.5 and 4.6 with focus on weak winds, June, July and August stand out as the months that experience fewest occasions with strong wind. This is verified by Figure 5.1, which shows the wind strength during the two years. The summer of 2008 experiences separate days of moderate wind, but overall relative calm conditions. The data for 2009 indicate in general a calm summer regarding the wind. To conclude that the wind are weaker during these months is too daring, but it can be viewed as a pointer.

The sea ice in the MIZ melts during both summer and winter, due to the proximity of water with temperatures above the freezing point, as described in Section 2.2.1. One of the main reasons why the melting increases during the summer months

are mainly because the solar radiation is at its most intense. This heating of the surface layer increases the melting potential.

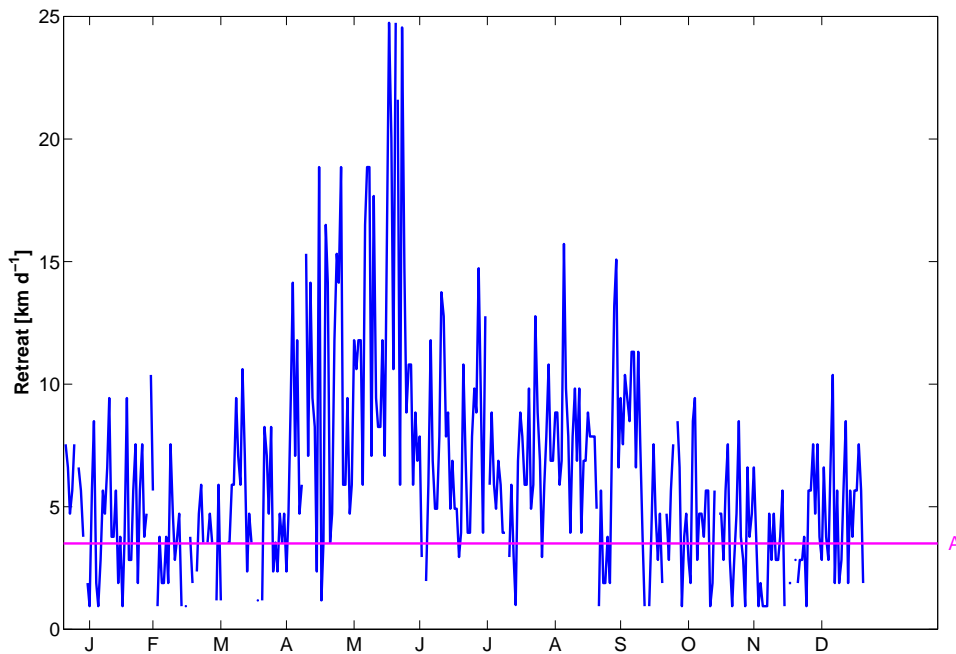


**Figure 5.1:** *The variation of the wind force with focus on the wind speed. The blue chart has data from 2008, the green shows the data from 2009.*

Some of the formation mechanisms are also affected by the season. During winter the water column becomes well mixed and fairly homogeneous due to the cooling in anticipation of freezing. The system is more barotropic due to less stratification. During summer, the sun heats the upper layers of the ocean, creating stronger baroclinicity and thus arranging the rise of eddies. The formation of open ocean eddies in the WSC is also affected by the heating and cooling, thus the number of advected eddies varies with the season.

In Figure 5.2 the seasonal variations of the different parameters of Equation 2.8 (discussed in Section 4.4) are multiplied with the number of eddies each month (from Table 4.1) to emphasize the seasonal variation of the retreat. The values of the parameters are adjusted to the conditions that reflect the season they belong to, the range can be found in Table 4.7. The mean retreat ( $A$ ) is also inserted, to emphasize the affect of the abundant eddies. The seasonal variation shows a resemblance to the trend shown by the eddy occurrence (e.g Figure 4.1); one can see an increase towards the end of April, reaching the peak in May-June, and then a decrease rest of the year. The slightly increase in retreat in December is

due to the increased number of eddies apparent.

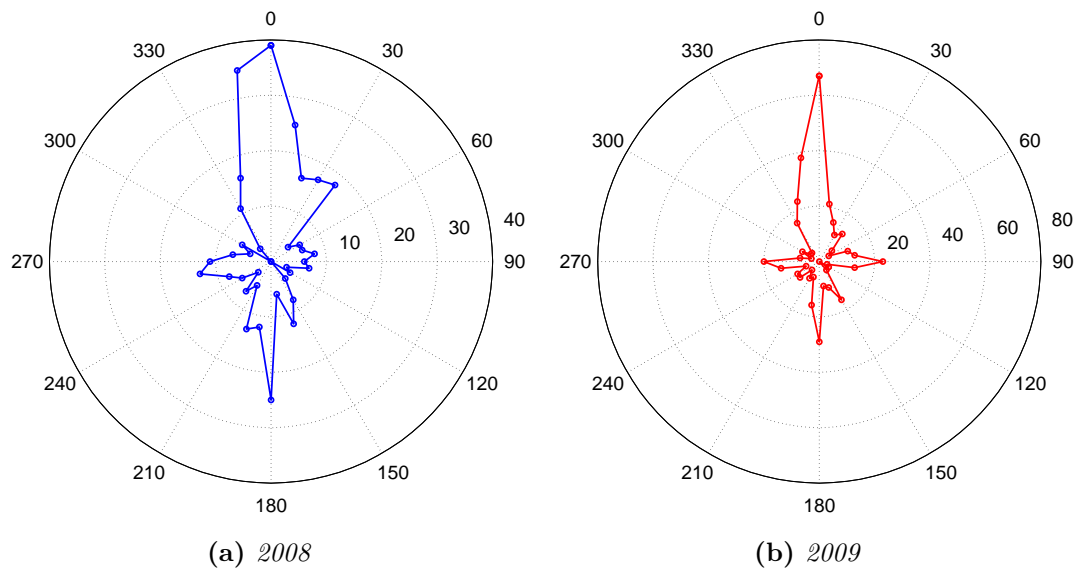


**Figure 5.2:** *The calculated retreat (by using Equation 2.8) multiplied with the number of eddies (Table 4.1) on the y-axis, plotted against the months on the x-axis. The pink line (A) denotes the calculated mean retreat. The data are from both 2008 and 2009.*

## 5.2 Wind influence

Eddy signature is evident in all wind directions, but most frequent occurrence is when the wind is directed from south or north, with a distinct predominance of the latter. The eddy occurrences are plotted against the wind direction in Figure 5.3 to support this conclusion. They show the same as Table 4.5 and 4.6, but in a more unifying way. Note the different scales on the two sub-figures.



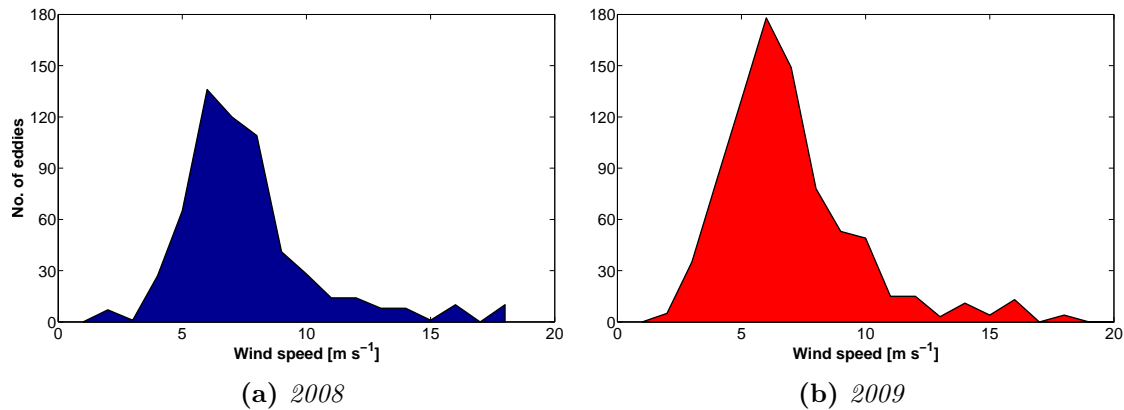


**Figure 5.3:** Eddy distribution in relation to wind direction. Note the different scales on the two figures. (a) has data from 2008, (b) has data from 2009.

To investigate the effect of the wind direction, the theory in Section 2.3.3 must be revisited. Two of the main wind directions are drawn in Figure 2.3. The Ekman theory states that when the wind blows with the coast on the right hand side (looking downwind), the transportation of water is directed towards the coast (Figure 2.3b). The converse finds place when the wind blows with the coast on the left hand side (Figure 2.3a). This suggests that northerly winds pack the ice, while southerly winds will shed the ice further offshore. Wind directed perpendicularly towards the ice edge will also have a packing effect, since the wind force will lead the ice towards the coast. In the opposite directed wind will contribute to shed the sea ice offshore. Some of the directions of the wind are thus expected to have a destroying effect on the presence of eddies.

It is obvious from Table 4.5 and 4.6 in addition to Figure 5.3 that the wind direction is not always destructive; the surface signature is evident in spite of non-favoured wind direction. One explanation might be a shift in the wind direction relatively recently. The method used to acquire the wind data does not include the history of the wind field.

When it comes to the wind speed, eddy occurrence is clearly most frequent in the low velocity area, but it is evident that a number of eddies exist at the high velocity area as well. Figure 5.4 express the number of eddies observed during different wind speeds. The favoured wind speed is around  $6-7 \text{ m s}^{-1}$ .



**Figure 5.4:** Number of eddy occurrences versus wind speed. (a) has data from 2008, (b) has data from 2009.

Intense wind forcing may destroy the expressions of upper ocean eddies relatively rapidly. For a couple examples one can study Figure 5.1 simultaneously with Figure 4.1. Strong wind in association with few eddy observations is evident in the beginning of May and in the end of June in 2008, and in the beginning of March and the end of April in 2009. The ice will respond to the wind during strong, uniform winds, while the sea ice will reflect the underlying ocean circulation during weaker winds.

The sea ice boundary might maintain the signature of an eddy while the drifting ice floes are shed off in response to strong winds. The boundary signature is regarded as an adequate eddy during data acquisition, in spite of erased clear ice convergence. This may explain some of the evident eddies in spite of strong winds. Another possible explanation may be that the wind has just recently gained strength so that the sea ice in the eddy has not yet been shed off. This is observed by McPhee *et al.* (1987), they study the ice movement in response to wind. It was found that the drift of sea ice and the wind velocities were closely correlated most of the time. However, in one occasion they observe a decline and shift in the wind field without changes in the ice.

It should be noted that HIRLAM has limited coverage in Area 3, and NCEP data are frequently missed. This makes the wind speed and -direction data incomplete in this area, as evident in the two tables in Appendix B.

## 5.3 Eddy cyclones versus anticyclones

The observed eddies are found to be predominantly cyclonic, 77% of the eddies observed rotate in the counter clockwise direction. This applies to both years.

This distinction between cyclones and anticyclones is a direct consequence of the barotropic shear that exists near the ice edge, as sketched in Figure 2.4 and discussed by Johannessen *et al.* (1987a). The ice edge jet that is formed during northerly wind (described in Section 2.2.1) will experience less friction further off the ice edge. The resulting shear favours cyclonic eddies. The velocity shear thus favours cyclonic eddies at the ice edge. Anticyclones are generated beneath the ice, and will appear at the surface only if the ice edge moves north or the eddy itself moves southward. Wind from the south favours anticyclonic eddies at the ice edge for the same reason. The prevailing currents and jets at the ice edge are directed towards the south-west. The wind data (Figure 5.3) also indicates a predominance of occasions with wind from the north, thus explaining the majority of cyclones.

In the Fram Strait region, the conservation of potential vorticity of the AW as it moves westward favours cyclonic rotation. This comprises the vortex stretching that result from increasing bottom depths. The theory of Häkkinen (1986) covering the ice-induced formation of eddies due to differential Ekman pumping (Section 2.4) also supports the majority of cyclonic eddies.

### Differential trapping

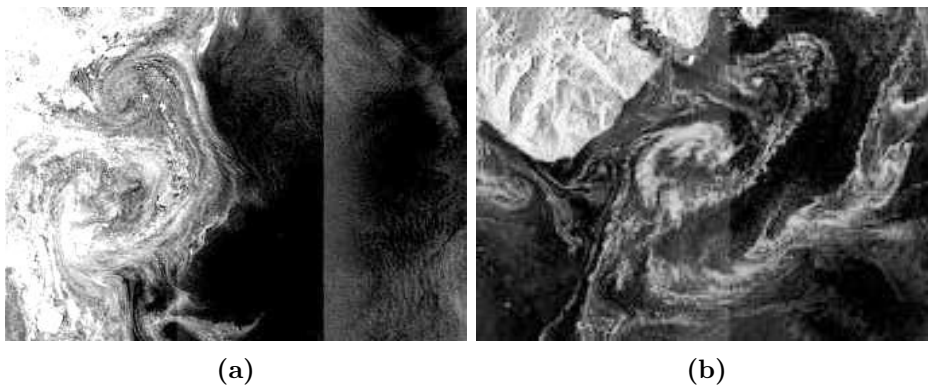
Early *et al.* (2011) show that quasi-geostrophic eddies can transport considerable amounts of fluid over long distances. The fluid in the eddy core remains there from the initialization region until the decay of the eddy. The outer ring does not have the same property, it entrains and shed fluid off during its life time.

The trapping of sea ice in an eddy are considered to be due to the spiraling motion described in Section 2.5.2 and figurative by Figure 2.6. The spiral structure drags the sea ice towards the eddy center in both cyclones and anticyclones. Other factors that contribute to the inward motion of sea ice are suggested to be ageostrophic effect, the surface tilt due to the rotation, and the Coriolis force.

It is expected that anticyclones contain more sea ice than cyclones (*cf.* Section Trapping). Examples of cyclones and anticyclones with both accumulation

and dispersion can be seen in Figure 4.5 and 4.6. One explanation for this obvious contradiction might be that the cyclone has been around longer and have had the ability to collect sea ice for a long time. A similar explanation is that the anticyclone has melted the ice in its centre efficiently. The temporal evolution of the eddy formation, growth and decay is the clue. The stage of the evolution will indeed manifest different amount of trapped ice.

A vortex pair consist of a cyclone and an anticyclone that are generated at the same time. A vortex pair will thus reveal which of the rotations that collects most sea ice in their centres. By taking a close inspection of the examples of vortex pairs in Figure 5.5a or 5.5b, one can see that the cyclones do contain less sea ice in the center compared to the anticyclonic part. The spiraling motion has worked on both the rotations for the same time, thus the asymmetry must be explained with reference to the ageostrophy.



**Figure 5.5:** *Two examples showing the difference of the amount of sea ice in the cyclonic and the anticyclonic part of a vortex pair. Both vortex pairs have a horizontal size of approximately  $20 \times 50$  km.*

## 5.4 The eddy induced melting

It is found that the sea ice in an eddy melts away in about 4 days. This calculation is based on a fixed bottom ablation and an assumed ice thickness. The eddy in Figure 4.8 does not by far melt all its ice in 4 days, it seems like it needs more than 20 days. This departure can be explained by the fact that eddies continue to accumulate sea ice continually during their operating time. The melting and trapping of sea ice happens simultaneously. The unimportance of the horizontal scale of the ice floe was mentioned previously. As long as the diameter of the ice floe is larger than the thickness of the ice, the period of time it takes to melt the

ice depends only on the thickness, due to the dominating bottom ablation. For an eddy containing ice floes with diameters above 3 m the complete melting will always take 4 days.

The calculation of the zonal retreat is based on considerations made around the five parameters of Equation 2.8, and is found to be  $3.5 \text{ km d}^{-1}$  per 100 km of ice edge. This correspond relatively well with the findings of (Johannessen *et al.*, 1987a), who report a value of 1 to 2  $\text{km d}^{-1}$ , per 50 km ice edge. The calculated retreat is about the twice of their findings, the explanation is that they used a mean eddy radius of 15 km, while the radius used here is 30 km.

Finally, the yearly melt of sea ice due to eddies is calculated to be  $0.7 \times 10^6 \text{ km}^2$ . When including the sea ice extent of 1000 km, the mean retreat of the ice edge becomes 700 km. By dividing this yearly loss of sea ice with the number of days during a year, one get  $\sim 2 \text{ km d}^{-1}$ , just as reported by Johannessen *et al.* (1987a).

The deviation from previous work can be explained by a number of factors. First of all, it should be noted that the values used for calculating the retreat (*cf.* Table 4.7) are based on *in situ* data retrieved in a confined area during the summer months, but are assumed to be representative for the whole year and the whole area. As already taken into consideration, the total number of 1000 eddies during a year must be viewed as an overestimation. By assuming that each eddy on average has been counted twice, the number of 500 is with certainty used in the calculations.

The size and the appurtenant amount of sea ice contained in an eddy does also imply some uncertainty. The volume of sea ice an eddy is capable of containing is calculated to be  $\sim 1.4$  to  $3 \text{ km}^3$ . As already mentioned, this is based on an estimated thickness and a fixed mean radius, and is thus a relative coarse calculation. The difference in cyclones and anticyclones is not included. Moreover, it is worth to consider if the final quantity of sea ice is achieved, or if the eddy still intercepts ice.

In the calculations it is assumed that the ice floes have a diameter of approximately 200 m, thus the conclusion that the bottom ablation is the main mechanism that contributes to the melting can be made. When the bottom ablation is the only mechanism that melts the sea ice, the effect of varying fraction of sea ice in an eddy can be omitted. The ocean heats the sea ice from below with an amount capable of melting  $0.38 \text{ m d}^{-1}$ . This emission of heat is independent of the sea ice above. This emphasize that it is the ice thickness that decide the time

period it takes to melt away the sea ice and not the horizontal scale, as briefly touched earlier in this section. This is not adequately addressed by Johannessen *et al.* (1987a). By assuming smaller ice floes, which is more realistic, the relation between the area of the bottom and the area of the sides shows that the ablation is dominated by lateral melting. The ice in an eddy is composed of ice floes with different sizes, so the lateral ablation should not be written off. The effect of the possible frictional force between ice floes in the eddy is not considered. Other factors that influence the melting in an eddy are the rotational speed of the eddy, how efficient the eddy can accumulate sea ice in its centre, and the length of the time period the eddy are present, and with that the wind conditions in relation to the wind field.

Other estimations of the ice edge retreat has been made in the area as well. The assumptions already discussed are assumed to also explain the deviation from the following results; Quadfasel *et al.* (1987) reports an enhanced zonal melt rate of  $5 \text{ km d}^{-1}$  due to the advection of warm AW in the Fram Strait (north of  $80^\circ \text{ N}$ ). It is worth mentioning that this is when the available heat is used on melting only. Vinje & Finnekåsa (1986) reports of a melt rate of  $0.5 \text{ km d}^{-1}$ , based on observations of four eddies in May 1976. According to Chiu *et al.* (1987, and references therein) the retreat of the ice edge could be reduced by a factor of ten without the presence of eddies. Energy considerations made by Manley (1987) indicate an ice edge retreat of  $0.2\text{-}0.6 \text{ km d}^{-1}$ . He assumed that all the available energy stored in the surface layer could be used to melt the ice, and that two eddies are present every 100 km. Foldvik *et al.* (1988) are sceptical to give eddies an important role regarding the melting of sea ice. They state that eddies do not contribute to the heat flux in the EGC with their small temperature anomalies. This paper is based on observations in the northern part of the EGC.

# CHAPTER 6

---

## Conclusion

---

In this thesis, eddies in the marginal ice zone in the Fram Strait, the Greenland Sea and the northern Denmark Strait have been studied using spaceborne Synthetic Aperture Radar (SAR) observations from the Envisat satellite operated by the European Space Agency (ESA). A total of 4000 SAR images collected from 2008 and 2009 have been investigated. The eddy characteristics have been arranged according to the spatial dimensions, rotational expressions, and frequency of existence versus wind field conditions. Following this, the importance of eddies for melting of sea ice and associated ice edge retreat has been investigated. The satellite SAR observations alone cannot be used to determine eddy formation mechanisms explicitly. Following previous work it is therefore assumed that they are formed by a mixture of generation mechanisms (baroclinic, barotropic and topographic) for eddies in the marginal ice zone area.

- The eddy radius range from 20-40 km.
- There is a prevailing majority of cyclonic eddies present. The ratio between cyclones to anticyclones is  $\sim 3:1$ .
- The presence of eddies in relation to the wind field shows that relative low wind speed and wind directed from the north favours the existence of eddy expression on the surface. However, eddies were found both during high wind speed and unfavourable wind direction. The history of the wind field and particular rapid wind shifts connected with polar lows etc (not examined here) is potentially a significant factor.

- The presence of eddies versus region indicate that 39% of the eddies are located in Area 1, 54% in Area 2, while only 7% is evident in Area 3. The seasonal variation of the location of the sea ice extent and the formation mechanisms were discussed as probable explanations.
- The presence of eddies versus season shows that summer and early fall are the peak seasons for eddies. This can be referred to the wind field data, which indicate corresponding seasonal variation. The formation mechanisms are affected by seasonal variations, as well.
- Assuming a sea ice fraction of 50%, an eddy is capable of carrying 1413.7 km<sup>2</sup> ice. Multiplying this with the assumed total of eddies during a year, it amounts to  $0.7 \times 10^6$  km<sup>2</sup>. The estimated volume of sea ice, based on a mean thickness of the ice of 1.5 m, becomes 2 km<sup>3</sup>
- An eddy is capable of melting all its ice content in four days. During its operating time it continually accumulates sea ice from the periphery and toward its centre while the melting are proceeding.
- The retreat of the ice edge is calculated by accounting for the bottom ablation ( $0.38 \text{ m d}^{-1}$ ), the eddy separation distance (assumed 100 km), the ice area calculated using a radius of 30 km and an assumed sea ice thickness of 1.5 m. On average, an eddy is able to melt  $3.5 \text{ km d}^{-1}$  of ice (per 100 km ice edge). With an ice edge of 1000 km, this results in a total of  $35 \text{ km d}^{-1}$ .

As the eddy expressions, number of eddies and the amount of ice trapped in them are determined subjectively, the results might be somewhat biased due to this. Some of the ASAR images have distinct and easy to classify eddy features while others contain vaguer eddy signatures. The total number of eddies might be underestimated due to this ambiguity. Furthermore, the possibility to count the same eddy several times is likely. An eddy moves southward with a speed of approximately  $10 \text{ km d}^{-1}$ , a fact that should also be taken into consideration when counting.

Moreover, the values and parameters used to quantify the retreat are retrieved from the MIZEX'83-84, carried out during the summer months in the Fram Strait. Their findings are assumed to be applicable for the entire year, and for the entire area. In addition, as satellite remote sensing only acquires surface expressions of the mesoscale eddies along the marginal ice zone, *in situ* measurements are needed to provide subsurface information of the water masses and the melting conditions along the MIZ.



All in all it would therefore be highly needed and desirable to execute a dedicated MIZ eddy field experiment. This in order to provide more reliable quantification of the influence of eddies of melting and sea ice retreat.



# APPENDIX A

---

## Abbreviations

---

AMSR-E	Advanced Microwave Scanning Radiometer
Area 1	The Fram Strait
Area 2	The Central and East Greenland Sea
Area 3	The Denmark Strait
ASAR	Advanced Synthetic Aperture Radar
AW	Atlantic Water
BB	Boreas Basin
CMOD-4	Algorithm used to calculate wind speed
CTD	Conductivity-Temperature-Depth
EGC	East Greenland Current
EM	Electromagnetic
ENVISAT	Environmental Satellite
EOS	Earth Observing System
ERS	European Remote Sensing Satellites (1 and 2)
ESA	European Space Agency
ECMWF	European Centre for Medium-Range Weather Forecasts
FY	First-Year
FZ	Fracture Zone
GB	Greenland Basin
GFS	Global Forecast System
GS	Greenland Sea
HIRLAM	High Resolution Limited Area Model
IR	Infra-Red

JM	Jan Mayen
MERIS	Medium-Resolution Imaging Spectrometer
MIZ	Marginal Ice Zone
MIZEX	Marginal Ice Zone Experiments
MODE-1	Mid-Ocean Dynamics Experiment
MY	Multi-Year
NASA	National Aeronautics and Space Administration
NCEP	National Centers for Environmental Predictions
NERSC	Nansen Environmental and Remote Sensing Center
NH	Northern Hemisphere
NwAC	Norwegian Atlantic Current
POLYGON-70	The first exp. to establish the existence of mesoscale eddies
POLYMODE	Polygon Mid-Ocean Dynamics Experiment
PW	Polar Water
SAR	Synthetic Aperture Radar
SB	Svalbard
SEASAT	First satellite observing Earth's ocean using SAR
SH	Southern Hemisphere
WSC	West Spitsbergen Current
WSM	Wide Swath Mode

# APPENDIX B

## Data

### B.1 The Data from 2008

Date	Area 1	Area 2	Area 3	Nr	Vel 1	Vel 2	Vel 3	Dir 1	Dir 2	Dir 3
1.1.	1	0	0	1	13			200		
2.1.	0	2	0	2		6			270	
4.1.	2	3	0	5	5	6		210	160	
5.1.	2	4	0	6	4	5		340	140	
7.1.	4	0	0	4	8			20		
8.1.	3	0	0	3	NaN			NaN		
11.1.	0	2	0	2		5			350	
13.1.	1	0	0	1	NaN			NaN		
14.1.	1	0	0	1	5			5		
20.1.	1	1	0	2	4	7		70	350	
21.1.	1	1	0	2	7	6		340	220	
22.1.	2	0	0	2	6			60		
23.1.	1	0	0	1	NaN			NaN		
24.1.	1	2	1	4	NaN	7	8	NaN	60	330
25.1.	0	2	0	2		6			10	
27.1.	1	0	0	1	5			30		
12.2.	0	1	0	1		7			340	
13.2.	0	1	0	1		5			350	
14.2.	1	1	0	2	10	10		220	220	
15.2.	0	2	0	2		7			300	
16.2.	0	1	0	1		4			330	
19.2.	0	2	0	2		7			150	

Continues on next page. . .

Table B.1 – Continued

Date	Area 1	Area 2	Area 3	Nr	Vel 1	Vel 2	Vel 3	Dir 1	Dir 2	Dir 3
20.2.	1	0	0	1	8			250		
21.2.	1	2	0	3	6	6		270	10	
22.2.	0	5	0	5		8			30	
23.2.	1	0	0	1	NaN			NaN		
25.2.	0	1	0	1		16			10	
27.2.	1	3	0	4	NaN	NaN		360	360	
28.2.	2	0	0	2	8			150		
2.3.	1	2	0	3	15	14		10	340	
3.3.	1	0	0	1	6			10		
4.3.	1	0	0	1	NaN			NaN		
6.3.	1	0	0	1	6			260		
7.3.	1	2	0	3	12	12		330	330	
8.3.	2	1	0	3	6	5		360	90	
10.3.	1	0	0	1	8			100		
11.3.	2	2	0	4	5	NaN		200	NaN	
16.3.	0	2	0	2	6			360		
17.3.	1	1	0	2	7	6		10	10	
18.3.	2	0	0	2	7			20		
19.3.	1	1	0	2	6	7		40	50	
20.3.	1	1	0	2	10	10		10	10	
21.3.	1	4	0	5	NaN	NaN		NaN	NaN	
22.3.	0	1	0	1		5			5	
26.3.	1	0	0	1	8			360		
29.3.	0	1	0	1		4			330	
1.4.	1	1	0	2	6	10		10	10	
2.4.	2	0	0	2	6			5		
4.4.	1	0	0	1	8			80		
5.4.	1	1	0	2	9	9		30	40	
7.4.	0	2	0	2		8			360	
8.4.	0	4	0	4		6			50	
9.4.	3	0	0	3	NaN			NaN		
10.4.	1	2	0	3	6	5		30	20	
11.4.	2	0	0	2	7			20		
13.4.	1	1	0	2	5	6		360	150	
14.4.	0	4	2	6		4	7		350	220
15.4.	4	0	0	4	NaN			NaN		
16.4.	2	6	0	8	7	8		360	180	
17.4.	0	2	0	2		5			360	
18.4.	4	0	0	4	5			NaN		
20.4.	0	3	2	5		2	7		360	220
21.4.	0	4	0	4		5			40	
22.4.	2	6	0	8	4	6		240	360	

Continues on next page...

Table B.1 – Continued

Date	Area 1	Area 2	Area 3	Nr	Vel 1	Vel 2	Vel 3	Dir 1	Dir 2	Dir 3
23.4.	0	4	0	4		9			360	
26.4.	0	5	0	5		7			140	
28.4.	0	3	0	3		NaN			NaN	
29.4.	0	2	0	2		8			360	
30.4.	2	0	0	2	8			360		
1.5.	0	2	0	2		7			80	
3.5.	1	0	0	1	5			350		
4.5.	2	2	0	4	7	2		210	160	
5.5.	1	2	0	3	10	6		190	350	
6.5.	1	2	0	3	8	4		320	350	
7.5.	1	2	0	3	NaN	NaN		NaN	NaN	
8.5.	3	1	0	4	16	12		30	20	
9.5.	1	2	0	3	18	18		360	360	
10.5.	0	0	1	1			10			40
11.5.	0	2	0	2		5			330	
12.5.	0	2	2	4		8	5		350	90
13.5.	1	2	0	3	6	4		280	240	
14.5.	0	4	0	4		NaN			10	
15.5.	2	3	0	5	4	4		300	300	
16.5.	2	0	0	2	6			10		
17.5.	2	4	0	6	9	6		360	360	
18.5.	1	2	0	3	6	7		10	340	
19.5.	3	4	0	7	8	5		10	360	
20.5.	2	0	0	2	6			350		
21.5.	1	6	1	8	5	6	7	270	10	30
23.5.	3	0	0	3	6			270		
25.5.	0	1	0	4		7			240	
26.5.	2	0	0	2	10			350		
27.5.	0	4	0	4		5			170	
28.5.	1	3	0	4	3	6		350	250	
29.5.	2	2	0	4	8	6		260	260	
30.5.	0	3	0	3	10	6		200	180	
31.5.	1	0	0	1	5			190		
1.6.	2	4	0	6	8	6		200	260	
2.6.	1	2	0	3	NaN	NaN		270	240	
3.6.	3	7	0	10	6	5		190	160	
4.6.	2	4	0	6	5	6		5	350	
5.6.	0	2	1	3		NaN	NaN	360	360	
6.6.	0	4	0	4		6			7	
7.6.	2	5	0	7	6	5		100	100	
9.6.	0	3	0	3		4			180	
10.6.	2	0	0	2	12			20		

Continues on next page. . .

Table B.1 – Continued

Date	Area 1	Area 2	Area 3	Nr	Vel 1	Vel 2	Vel 3	Dir 1	Dir 2	Dir 3
11.6.	0	1	2	3		4	5		340	250
12.6.	0	2	0	2		7			20	
14.6.	0	0	2	2			5			160
15.6.	2	4	0	6	6	7		350	80	
16.6.	0	4	1	5		8	7		30	80
17.6.	2	0	0	2	7			350		
20.6.	1	0	1	2	6		8	290		200
21.6.	4	5	0	9	7	8		60	350	
22.6.	1	7	0	8	8	9		10	350	
23.6.	1	4	0	5	14	5		350	9	
24.6.	2	5	0	7	6	8		40	30	
25.6.	0	3	1	4		9	10		340	360
26.6.	1	2	0	3	12	12		360	360	
27.6.	0	3	0	3		NaN			360	
29.6.	0	3	0	3		6			5	
1.7.	0	7	0	7		5			250	
3.7.	0	2	0	2		4			190	
5.7.	0	2	0	2		9			180	
6.7.	3	1	0	4	8	5		5	290	
7.7.	0	4	0	4		10			20	
8.7.	0	4	0	4		7			350	
9.7.	2	1	0	3	7	8		300	260	
10.7.	0	1	0	1		5			350	
11.7.	0	5	0	5		7			200	
13.7.	1	2	0	3	8	5		160	210	
14.7.	0	0	2	2			7			80
15.7.	0	4	0	4		5			40	
16.7.	3	0	0	3	8			40		
17.7.	3	2	0	5	7	8		60	360	
18.7.	2	0	0	2	8			5		
19.7.	2	1	0	3	5	NaN		5	340	
20.7.	0	3	0	3		8			190	
22.7.	0	2	0	2		6			350	
23.7.	4	1	0	5	5	4		340	360	
24.7.	0	3	0	3		5			180	
25.7.	1	0	0	1	7			200		
26.7.	2	4	0	6	6	5		260	180	
27.7.	3	4	0	7	6	7		250	190	
28.7.	3	2	0	5	8	9		180	200	
29.7.	0	3	0	3		5			290	
30.7.	1	1	0	2	4	6		350	240	
31.7.	5	1	0	6	7	6		200	260	

Continues on next page...



Table B.1 – Continued

Date	Area 1	Area 2	Area 3	Nr	Vel 1	Vel 2	Vel 3	Dir 1	Dir 2	Dir 3
3.8.	5	2	0	7	2	6		360	40	
4.8.	5	2	0	7	8	7		360	20	
5.8.	1	3	0	4	6	5		30	350	
7.8.	1	1	0	2	6	4		280	360	
8.8.	0	2	0	2		6			210	
9.8.	4	0	0	4	9			30		
12.8.	3	2	0	5	5	8		40	330	
13.8.	1	0	0	1	14			280		
14.8.	1	1	0	2	9	7		150	180	
15.8.	0	2	0	2		6			90	
16.8.	4	5	0	11	7	7		350	330	
17.8.	6	0	0	6	6			230		
18.8.	2	0	0	2	7			260		
20.8.	3	1	0	4				140	180	
21.8.	5	1	0	6	5	4		180	290	
22.8.	4	0	0	4	7			170		
23.8.	2	4	0	6	5	7		300	90	
24.8.	0	2	0	2		6			80	
25.8.	0	2	0	2		9			110	
26.8.	3	0	0	3	8			120		
27.8.	4	3	0	7	NaN	NaN		180	140	
28.8.	3	0	0	3	5			80		
29.8.	3	2	0	5	6	7		10	40	
30.8.	3	2	0	5	9	8		280	270	
31.8.	0	1	0	1		5			300	
2.9.	2	3	0	5	7	7		180	180	
5.9.	1	2	0	3	7	6		10	180	
7.9.	4	0	0	4	7			150		
8.9.	4	6	0	10	7	6		160	180	
9.9.	6	6	0	12	9	7		200	180	
10.9.	4	0	0	4	7			230		
11.9.	4	3	0	7	7	6		240	190	
12.9.	1	3	0	4	12	11		160	160	
13.9.	3	5	0	8	7	11		250	170	
14.9.	3	3	0	6	8	7		190	200	
15.9.	2	5	0	7	11	NaN		190	160	
16.9.	7	4	0	11	11	13		170	180	
17.9.	5	6	0	11	10	8		270	120	
18.9.	1	6	0	7	9	8		160	110	
19.9.	6	4	0	10	9	6		100	160	
20.9.	5	3	0	8	6	8		160	70	
21.9.	2	2	0	4	5	10		340	340	

Continues on next page. . .

Table B.1 – Continued

Date	Area 1	Area 2	Area 3	Nr	Vel 1	Vel 2	Vel 3	Dir 1	Dir 2	Dir 3
22.9.	1	0	0	1	9			5		
24.9.	1	0	0	1	6			5		
25.9.	0	3	0	3	0	10			70	
26.9.	1	4	0	5	8	6		230	250	
27.9.	4	1	0	5	4	7		10	330	
28.9.	3	0	0	3	6			60		
29.9.	1	3	0	4	14	14		20	20	
30.9.	1	1	0	2	7	9		30	20	
2.10.	2	0	0	2	8			10		
3.10.	0	3	0	3		5			200	
4.10.	1	0	0	1	5			260		
5.10.	3	5	0	8	8	6		270	350	
7.10.	5	4	0	9	6	7		150	180	
8.10.	1	3	0	4	7	8		270	210	
9.10.	0	1	0	1		10			220	
10.10.	3	1	0	4	8	6		260	50	
11.10.	2	3	0	5	6	16		280	360	
12.10.	2	1	0	3	10	14		340	360	
13.10.	1	0	0	1	7			330		
14.10.	0	4	0	4		7			280	
15.10.	2	0	0	2	6			270		
17.10.	0	3	0	3		9			20	
18.10.	0	1	0	1		NaN			10	
19.10.	4	0	0	4	9			40		
20.10.	1	3	0	4	10	5		360	5	
21.10.	1	0	0	1	8			5		
24.10.	2	0	0	2	8			70		
26.10.	1	0	0	1	6			30		
27.10.	1	0	0	1	10			20		
28.10.	1	2	0	3	7	6		40	80	
29.10.	0	5	0	5		7			40	
30.10.	1	6	0	7	6	7		260	150	
31.10.	2	1	0	3	16	18		120	180	
2.11.	1	5	0	6	10	14		40	330	
3.11.	0	0	2	2			12			270
4.11.	1	2	4	7	7	4	5	30	340	360
5.11.	0	3	0	3		9			360	
6.11.	0	1	0	1		NaN			NaN	
7.11.	1	0	0	1	8			5		
8.11.	0	3	0	3		NaN			350	
9.11.	2	0	0	2	7			40		
10.11.	1	0	0	1	18			70		

Continues on next page...

Table B.1 – Continued

Date	Area 1	Area 2	Area 3	Nr	Vel 1	Vel 2	Vel 3	Dir 1	Dir 2	Dir 3
11.11.	0	3	0	3		12			350	
15.11.	1	0	0	1	9			5		
18.11.	1	1	1	3	8	NaN	NaN	30	120	100
20.11.	0	1	2	3		8	5		350	360
21.11.	0	0	1	1			NaN			340
22.11.	1	0	0	1	5			190		
23.11.	1	2	0	3	8	7		190	180	
24.11.	0	2	2	4		6	14		170	200
25.11.	1	0	0	1	NaN			NaN		
27.11.	0	1	0	1		8			350	
30.11.	2	0	0	2	6			10		
1.12.	1	0	0	1	8			360		
2.12.	3	0	0	3	7			40		
3.12.	0	2	0	2		7			30	
4.12.	1	0	0	1	8			320		
6.12.	0	2	0	2		7			190	
7.12.	3	0	0	3	8			50		
8.12.	3	1	0	4	16	18		350	350	
9.12.	0	1	0	1	13			360		
10.12.	2	1	1	4	6	NaN	NaN	170	180	180
11.12.	2	0	0	2	6			40		
12.12.	3	0	0	3	8			110		
13.12.	4	0	0	4	6			10		
15.12.	1	0	0	1	10			150		
16.12.	2	2	0	4	8	7		60	40	
17.12.	4	2	0	6	6	8		90	70	
18.12.	0	2	0	2		12			20	
19.12.	2	2	0	4	18	12		360	350	
20.12.	0	2	0	2		10			350	
21.12.	3	0	0	3	9			350		
22.12.	0	4	1	5		8	6		100	100
23.12.	3	4	1	7	10	NaN	NaN	180	180	90
24.12.	1	1	0	2	10	10		180	220	
25.12.	2	3	1	6	5	9	7	30	340	250
26.12.	0	2	0	2		4			260	
27.12.	0	4	0	4		6			260	
28.12.	2	2	0	4	10	8		5	20	
29.12.	1	4	2	7	NaN	11	5	280	30	10
30.12.	1	2	0	3	12	12		350	350	
31.12.	1	1	0	2	8	6		320	340	

## B.2 The Data from 2009

Date	Area 1	Area 2	Area 3	Nr	Vel 1	Vel 2	Vel 3	Dir 1	Dir 2	Dir 3
1.1.	0	3	4	7		NaN	NaN		170	230
2.1.	2	3	0	5	10	5		360	50	
3.1.	2	3	0	5	12	7		360	250	
4.1.	1	0	0	1	12			360		
5.1.	0	2	0	2		10			330	
7.1.	0	0	3	3			7			260
8.1.	1	1	1	3	8	7	6	340	350	30
9.1.	3	1	0	4	13	6		360	10	
12.1.	0	1	0	1		8			340	
13.1.	1	4	0	5	7	6		280	270	
14.1.	2	2	0	4	6	6		210	220	
15.1.	0	2	0	2		8			40	
16.1.	0	1	0	1		12			90	
17.1.	3	0	0	3	7			70		
18.1.	3	3	0	6	6	5		150	90	
19.1.	2	2	1	5	5	5	8	160	90	80
20.1.	2	3	0	5	5	4		160	14	
21.1.	2	6	0	8	6	7		60	20	
22.1.	2	0	0	2	11			5		
23.1.	2	1	0	3	10	6		360	5	
24.1.	1	1	0	2	8	7		30	10	
26.1.	3	0	1	4	8		6	180		40
28.1.	3	1	0	4	10	9		170	180	
29.1.	3	5	2	10	4	4	5	260	360	350
30.1.	0	3	0	3		3			270	
31.1.	3	0	0	3	7			300		
1.2.	0	4	2	6		7	7		280	360
2.2.	3	5	0	8	8	8		240	350	
3.2.	0	2	0	2		20			360	
4.2.	2	1	3	6	10	7	NaN	100	80	NaN
5.2.	3	4	1	8	8	9	8	120	150	350
6.2.	0	4	0	4		7			120	
7.2.	5	0	0	5	6			160		
9.2.	4	7	0	11	6	6		40	80	
10.2.	3	3	0	6	18	16		360	10	
13.2.	1	2	0	3	12	12		350	350	
16.2.	0	3	0	3		10			160	
17.2.	0	0	2	2			10			150
18.2.	0	6	2	8		7	9		360	180
19.2.	1	2	0	3	10	8		360	350	

Continues on next page...

Table B.2 – Continued

Date	Area 1	Area 2	Area 3	Nr	Vel 1	Vel 2	Vel 3	Dir 1	Dir 2	Dir 3
20.2.	0	2	0	2		20			350	
21.2.	0	0	1	1	7		14			30
28.2.	1	5	0	6		9		270	280	
1.3.	2	0	0	2	8			40		
2.3.	1	0	0	1	16			100		
3.3.	1	2	0	3	5	NaN		40	5	
4.3.	2	0	0	2	16			360		
6.3.	0	2	0	2		NaN		360		
7.3.	0	1	0	1		16			10	
11.3.	1	0	0	1	10			350		
12.3.	1	0	0	1	5			30		
15.3.	1	2	0	3	6	5		330	70	
16.3.	0	1	0	1		4			10	
17.3.	1	2	0	3	NaN	NaN		NaN	NaN	
18.3.	2	1	0	3	16	4		360	90	
19.3.	2	4	0	6	3	9		360	340	
20.3.	1	3	0	4	9	5		350	10	
22.3.	0	6	2	8		7	NaN		30	70
23.3.	2	4	0	6	12	14		360	350	
24.3.	1	1	0	2	12	12		20	20	
25.3.	1	3	0	4	4	10		350	340	
26.3.	0	2	0	2		13			5	
31.3.	1	0	0	1	5			340		
1.4.	2	3	0	5	7	7		310	240	
2.4.	2	2	0	4	8	7		290	270	
3.4.	0	4	0	4		8			20	
4.4.	1	5	0	6	4	7		50	30	
6.4.	0	1	2	3		14	7		10	10
10.4.	0	1	0	1		13			360	
12.4.	1	1	2	4	8	7	6	310	280	240
13.4.	2	3	2	7	5	7	6	5	360	330
14.4.	1	5	0	6	12	9		350	360	
15.4.		2	0	2		14			20	
16.4.	1	1	0	2	16	8		360	5	
17.4.	0	2	0	2		14			330	
18.4.	1	0	0	1	18			340		
20.4.	2	3	3	8	8	9	8	350	320	160
21.4.	1	1	0	2	14	10		330	5	
22.4.	0	3	1	4		4	5		360	360
23.4.	2	2	0	4	8	6		260	360	
24.4.	3	4	0	7	7	9		330	5	
25.4.	1	0	1	2	3		3	90		10

Continues on next page. . .

Table B.2 – Continued

Date	Area 1	Area 2	Area 3	Nr	Vel 1	Vel 2	Vel 3	Dir 1	Dir 2	Dir 3
26.4.	5	3	3	11	6	5	7	340	60	10
27.4.	0	1	0	1		10			50	
29.4.	4	5	3	12	8	9	6	200	170	80
30.4.	5	4	1	10	5	8	9	340	150	90
1.5.	1	0	0	1	2			190		
2.5.	0	4	0	4		7			40	
3.5.	3	6	0	9	NaN	7		NaN	100	
4.5.	1	4	4	9	9	7	8	150	150	80
5.5.	0	6	3	9		6	7		5	5
6.5.	4	7	2	13	6	7	6	100	20	40
7.5.	0	2	0	2		9			90	
8.5.	1	0	0	1	7			80		
9.5.	2	3	0	5	5	10		80	20	
10.5.	1	2	0	3	9	7		180	350	
11.5.	2	1	0	3	10	8		200	190	
12.5.	2	4	0	6	8	6		260	250	
13.5.	3	3	0	6	14	7		260	250	
14.5.	3	3	0	6	7	5		270	270	
15.5.	0	5	0	5		7			230	
16.5.	1	4	0	5	9	11		290	270	
17.5.	5	3	0	8	7	3		190	200	
18.5.	0	10	3	13		6	NaN		180	180
19.5.	3	6	0	9	6	11		180	190	
20.5.	2	2	0	4	7	6		220	220	
21.5.	1	3	3	7		7	6	250	190	180
22.5.	4	3	1	8	4	8	7	260	230	190
23.5.	1	3	0	4	NaN	9		NaN	20	
24.5.	0	6	1	7		4	7		360	20
25.5.	0	7	2	8		5	12		20	5
26.5.	2	2	0	4	7	6		270	300	
27.5.	0	9	0	9		4			260	
28.5.	4	11	2	17	5	6	8	240	180	90
29.5.	5	8	0	13	5	6		NaN	270	
30.5.	3	3	0	6	8	5		210	180	
31.5.	3	14	3	20	4	5	10	360	270	190
1.6.	7	7	2	16	7	7	9	360	350	180
2.6.	1	0	2	3	3		6	5		210
3.6.	4	8	3	15	6	5	8	340	360	50
4.6.	2	6	1	9	10	10	6	350	360	100
5.6.	2	4	0	6	10	10		360	360	
6.6.	1	5	1	7	8	4	5	360	360	250
7.6.	0	4	0	4		7			360	

Continues on next page...

Table B.2 – Continued

Date	Area 1	Area 2	Area 3	Nr	Vel 1	Vel 2	Vel 3	Dir 1	Dir 2	Dir 3
8.6.	0	3	3	6		7	6		350	210
9.6.	0	4	2	6		5	4		180	190
10.6.	1	4	0	5	2	5		330	80	
11.6.	0	5	0	5		4			330	
12.6.	0	0	1	1			7			190
16.6.	3	4	0	7	4	7		5	350	
17.6.	3	2	0	5	7	10		90	270	
18.6.	2	3	0	5	6	7		100	170	
19.6.	0	4	1	5		7	6		30	230
20.6.	1	5	0	6	4	6		30	100	
21.6.	1	2	2	5	5	4	4	330	100	80
22.6.	2	3	0	5	6	8		150	60	
23.6.	3	0	0	3	4			70		
24.6.	2	0	0	2	6			120		
25.6.	0	1	0	1		7			210	
26.6.	3	1	0	4	6	6		270	240	
27.6.	0	2	0	2		7			230	
28.6.	2	2	1	5	4	2	5	270	180	240
30.6.	1	3	0	4	6	3		270	240	
1.7.	2	2	0	4	7	5		360	180	
2.7.	3	4	0	7	4	7		340	90	
3.7.	0	2	0	2		5			150	
4.7.	3	1	0	4	6	3		5	350	
5.7.	1	5	0	6	4	5		340	150	
6.7.	2	4	0	6	7	6		340	180	
7.7.	2	2	1	5	5	3	6	340	350	230
8.7.	3	7	1	11	6	6	11	270	190	230
9.7.	3	4	0	7	7	5		270	110	
10.7.	1	2	0	3	6	6		260	80	
11.7.	4	4	0	8	3	6		190	180	
12.7.	2	5	0	7	7	6		360	10	
13.7.	1	2	0	3	4	6		70	70	
14.7.	3	4	0	7	5	4		360	350	
15.7.	1	1	0	2	6	4		350	350	
16.7.	1	1	0	2	10	8		340	330	
17.7.	1	1	0	2	10	4		360	350	
18.7.	1	2	1	4	6	7	6	310	290	30
19.7.	0	1	0	1		6			360	
20.7.	0	1	0	1		4			320	
22.7.	1	0	0	1	10			40		
23.7.	0	1	0	1		6			50	
26.7.	1	0	0	1	2			180		

Continues on next page. . .

Table B.2 – Continued

Date	Area 1	Area 2	Area 3	Nr	Vel 1	Vel 2	Vel 3	Dir 1	Dir 2	Dir 3
27.7.	1	1	0	2	4	5		120	90	
28.7.	2	1	0	3	4	5		30	20	
29.7.	1	2	0	3	5	4		70	90	
30.7.	1	3	0	4	4	3		NaN	NaN	
31.7.	2	2	0	4	7	5		NaN	NaN	
1.8.	4	1	0	5	5	4		190	90	
2.8.	2	4	0	6	5	4		190		
3.8.	3	3	0	6	3	4		5	360	
4.8.	2	0	0	2	3			260		
5.8.	1	2	0	3	5	3		270	150	
6.8.	0	3	0	3		6			180	
7.8.	4	0	0	4	6			140		
8.8.	4	2	0	6	5	4		210	170	
9.8.	2	5	0	7	3	4		180	160	
10.8.	5	2	0	7	5	4		190	170	
11.8.	4	3	0	7	6	6		100	70	
12.8.	4	0	0	4	7			5		
13.8.	2	6	0	8	7	9		340	320	
14.8.	0	4	0	4		6			180	
15.8.	3	2	0	5	6	5		160	5	
16.8.	3	4	0	7	5	6		360	110	
17.8.	3	1	0	4	8	6		360	350	
18.8.	1	5	0	6	8	5		5	280	
19.8.	1	3	0	4	7	9		350	200	
20.8.	0	4	0	4		7			90	
21.8.	2	2	0	4	7	6		110	5	
22.8.	1	2	0	3		9			100	
23.8.	0	4	0	4		4			230	
24.8.	2	0	0	2		3			240	
25.8.	3	2	0	5	4	7		140	150	
26.8.	4	0	0	4	6			40		
27.8.	2	0	0	2	7			80		
28.8.	2	3	0	5	5	7		360	270	
29.8.	2	0	0	2	6			90		
30.8.	2	1	0	3	6	7		5	40	
31.8.	2	2	0	4	10	9		350	340	
1.9.	0	1	0	1		10			360	
2.9.	0	1	0	1		7			20	
3.9.	0	2	0	2		6			340	
4.9.	0	2	0	2		7			330	
5.9.	1	0	0	1	6			260		
6.9.	1	1	0	2	7	7		210	180	

Continues on next page...



Table B.2 – Continued

Date	Area 1	Area 2	Area 3	Nr	Vel 1	Vel 2	Vel 3	Dir 1	Dir 2	Dir 3
7.9.	1	3	0	4	5	9		330	10	
8.9.	1	2	0	3	7	6		260	180	
9.9.	2	2	0	4	6	5		350	30	
10.9.	1	2	0	3	6	9		340	200	
11.9.	3	0	0	3	7			150		
12.9.	4	0	0	4	NaN			NaN		
13.9.	2	1	0	3	11	NaN		350	NaN	
14.9.	2	2	0	4	10	14		230	360	
15.9.	2	0	0	2	7			360		
16.9.	0	1	0	1		16			330	
17.9.	1	0	0	1	10			330		
19.9.	0	2	0	2		7			10	
25.9.	1	0	0	1	6			180		
26.9.	2	1	0	1	10	15		20	360	
29.9.	0	1	0	1		16			360	
2.10.	0	3	0	3		NaN			NaN	
4.10.	0	5	0	5		5			310	
5.10.	0	4	0	4		8			350	
8.10.	0	3	0	3		8			300	
13.10.	1	0	0	1	16			180		
14.10.	0	4	1	5		6	4		190	90
15.10.	1	7	0	8	5	6			190	350
16.10.	1	2	0	3	7	8		360	220	
17.10.	1	1	0	2	7	5		90	360	
18.10.	2	1	1	4	6	8	16	360	360	350
20.10.	0	0	2	2			5			280
21.10.	0	1	4	5		9	NaN		260	NaN
22.10.	0	1	0	1		10			10	
23.10.	2	0	0	2	4			260		
24.10.	2	0	2	4	7		7	270		360
26.10.	2	0	2	4	7		6	360		40
27.10.	1	0	3	4	5		9	40		40
29.10.	1	0	0	1	10			360		
30.10.	0	0	1	1			18			360
1.11.	1	0	0	1	6			340		
2.11.	2	0	1	3	5		5	300		360
3.11.	2	1	0	3	5	4		320	10	
5.11.	2	0	0	2	11			300		
5.11.	1	0	0	1	5			280		
6.11.	1	1	0	2	6	4		170	90	
8.11.	3	0	1	4	6		3	10		360
9.11.	2	0	0	2	9			180		

Continues on next page. . .

Table B.2 – Continued

Date	Area 1	Area 2	Area 3	Nr	Vel 1	Vel 2	Vel 3	Dir 1	Dir 2	Dir 3
10.11.	2	1	0	3	11	15		150	150	
11.11.	2	2	0	4	14	10		160	170	
12.11.	3	1	0	4	5	4		340	300	
13.11.	1	0	0	1	7			10		
14.11.	1	1	0	2	9			360		
16.11.	1	0	0	1	10			60		
17.11.	0	1	0	1		12			360	
18.11.	0	1	1	2		7			90	
19.11.	3	0	0	3	5			180		
20.11.	1	1	0	2	7	7		100	90	
21.11.	1	1	0	2	4	7		90	50	
22.11.	1	1	0	2	7	9		340	350	
23.11.	1	0	0	1	7			360		
24.11.	1	0	1	2	9		14	360		10
27.11.	0	0	1	1			16			360
28.11.	0	0	2	2			18			360
30.11.	0	0	1	1			18			360
1.12.	0	0	1	1			20			350
3.12.	1	0	0	1	7			150		
4.12.	2	1	0	3	6	12		90	180	
5.12.	0	1	0	1		4			90	
6.12.	2	2	0	4	6	7		20	270	
7.12.	0	3	0	3		6			180	
8.12.	1	3	0	4	6	7		170	100	
9.12.	3	1	0	4	9	8		160	140	
10.12.	2	2	0	4	5	4		80	70	
11.12.	1	1	0	2	7	4		10	360	
13.12.	1	2	0	3	7	4		160	350	
14.12.	1	2	1	4	6	5	4	140	260	180
15.12.	1	1	0	2	3	5		100	340	
16.12.	1	0	2	3	8		6	200		240
17.12.	1	2	2	5	8	8	12	150	330	360
19.12.	1	0	1	2	16	6	7	350		10
22.12.	1	0	0	1	7			80		
23.12.	1	0	0	1	6			70		
26.12.	2	0	0	2	6			70		
27.12.	1	1	0	2	10	12		360	330	
28.12.	2	0	0	2	10			20		
29.12.	1	0	0	1	12			10		
30.12.	1	1	1	3	5	10	7	350	300	340

---

## References

---

- Aagaard, K., & Coachman, L.K. 1968. The East Greenland Current north of Denmark Strait, I. *Arctic*, **21**(3), 181–200.
- Berens, P. 2011 (April). *Introduction to Synthetic Aperture Radar (SAR)*. [http://www.sse.gr/NATO/EreunaKaiTexnologiaNATO/8.Advanced\\_radar\\_systems\\_signal\\_and\\_data\\_processing/RTO-EN-SET-086/EN-SET-086-03.pdf](http://www.sse.gr/NATO/EreunaKaiTexnologiaNATO/8.Advanced_radar_systems_signal_and_data_processing/RTO-EN-SET-086/EN-SET-086-03.pdf).
- BODC, (British Oceanographic Data Centre). 2010 (October). *General Bathymetric Chart of the Oceans*. <http://www.gebco.net/>.
- Brown, E., Colling, A., Park, D., Phillips, J., Rothery, S., & Wright, J. 2001. *Ocean circulation*. WH, Milton Keynes, United Kingdom: The Open University.
- Carmack, E.C. 1990. *Polar Oceanography, Part A: Physical Science*. Academic press. Chap. Large-scale physical oceanography of polar oceans, pages 171–221.
- Chiu, C.S., Lynch, J.F., & Johannessen, O.M. 1987. Tomographic resolution of mesoscale eddies in the marginal ice zone: A preliminary study. *Journal of Geophysical Research*, **92**(C7), 6886–6902.
- Cushman-Roisin, B., & Beckers, J-M. 2009. *Introduction to geophysical fluid dynamics*. Prentice Hall.
- Early, J.J., Samelson, R.M., & Chelton, D.B. 2011. The Evolution and Propagation of Quasigeostrophic Ocean Eddies. *Journal of Physical Oceanography*.
- Foldvik, A., Aagaard, K., & Tørresen, T. 1988. On the velocity field of the East Greenland Current. *Deep Sea Research Part A. Oceanographic Research Papers*, **35**(8), 1335–1354.

- Gascard, J.C., Kergomard, C., Jeannin, P.F., & Fily, M. 1988. Diagnostic study of the Fram Strait marginal ice zone during summer from 1983 and 1984 Marginal Ice Zone Experiment Lagrangian observations. *Journal of Geophysical Research*, **93**(C4), 3613–3641.
- Griffiths, R.W., & Linden, P.F. 1982. Laboratory experiments on fronts. *Geophysical & Astrophysical Fluid Dynamics*, **19**(3), 159–187.
- Häkkinen, S. 1986. Coupled ice-ocean dynamics in the marginal ice zones: Upwelling/downwelling and eddy generation. *Journal of Geophysical Research*, **91**(C1), 819–832.
- Hall, R.T., & Rothrock, D.A. 1987. Photogrammetric observations of the lateral melt of sea ice floes. *Journal of Geophysical Research*, **92**(C7), 7045–7048.
- Hanzlick, D.J. 1983. *The West Spitsbergen Current: transport, forcing, and variability*. Ph.D. thesis.
- HIRLAM. 2010 (October). *Phage Lambda: description & restriction map*. <http://hirlam.org/>.
- Huppert, H.E., & Bryan, K. 1976. Topographically generated eddies\*. *Pages 655–679 of: Deep Sea Research and Oceanographic Abstracts*, vol. 23. Elsevier.
- Ivanov, A.Y., & Ginzburg, A.I. 2002. Oceanic eddies in synthetic aperture radar images. *Journal of Earth System Science*, **111**(3), 281–295.
- Johannessen, J.A. 2011 (May). Personal communication.
- Johannessen, J.A., Johannessen, O.M., Svendsen, E., Shuchman, R., Manley, T., Campbell, W.J., Josberger, E.G., Sandven, S., Gascard, J.C., Olaussen, T., *et al.* 1987a. Mesoscale eddies in the Fram Strait marginal ice zone during the 1983 and 1984 Marginal Ice Zone Experiments. *Journal of Geophysical Research*, **92**(C7), 6754–6772.
- Johannessen, J.A., Shuchman, R.A., Digranes, G., Lyzenga, D.R., Wackerman, C., Johannessen, O.M., & Vachon, P.W. 1996. Coastal ocean fronts and eddies imaged with ERS 1 synthetic aperture radar. *Journal of geophysical research*, **101**(C3), 6651–6667.
- Johannessen, O.M., Johannessen, J.A., Morison, J., Farrelly, B.A., & Svendsen, E.A.S. 1983. Oceanographic conditions in the marginal ice zone north of Sval-

- 
- bard in early fall 1979 with an emphasis on mesoscale processes. *Journal of Geophysical Research*, **88**(C5), 2755–2769.
- Johannessen, O.M., Johannessen, J.A., Svendsen, E., Shuchman, R.A., Campbell, W.J., & Josberger, E. 1987b. Ice-edge eddies in the Fram Strait marginal ice zone. *Science*, **236**(4800), 427.
- Josberger, E.G. 1987. Bottom ablation and heat transfer coefficients from the 1983 Marginal Ice Zone Experiments. *Journal of Geophysical Research*, **92**(C7), 7012–7016.
- Kundu, P.K. 1990. *Fluid Mechanics*. San Diego, California: Academic Press.
- Manley, T.O. 1987. Effects of sub-ice mesoscale features within the marginal ice zone of Fram Strait. *Journal of Geophysical Research*, **92**(C4), 3944–3960.
- Maslowski, W., Roman, R., & Kinney, J.C. 2008. Effects of mesoscale eddies on the flow of the Alaskan Stream. *Journal of Geophysical Research*, **113**(C7), C07036.
- Maykut, G.A. 1978. Energy exchange over young sea ice in the central Arctic. *Journal of Geophysical Research*, **83**(C7), 3646–3658.
- McCandless, S.W., & Jackson, C.R. 2004. Principles of Synthetic Aperture Radar. *Synthetic Aperture Radar, Marine User's Manual*, 1–23.
- McPhee, M.G., Maykut, G.A., & Morison, J.H. 1987. Dynamics and thermodynamics of the ice/upper ocean system in the marginal ice zone of the Greenland Sea. *Journal of Geophysical Research*, **92**(C7), 7017–7031.
- Munk, W., Armi, L., Fischer, K., & Zachariassen, F. 2000. Spirals on the sea. *Proceedings: Mathematics, Physical and Engineering Sciences*, **456**(1997), 1217–1280.
- NOAA, (National Oceanic and Atmospheric Administration). 2011 (April). *National Centers for Environmental Predictions*. <http://www.ncep.noaa.gov/>.
- Pedlosky, J. 1987. *Geophysical fluid dynamics*. Springer.
- Proudman, J. 1916. On the motion of solids in a liquid possessing vorticity. *Proceedings of the Royal Society of London. Series A, Containing Papers of a Mathematical and Physical Character*, **92**(642), 408–424.

- Quadfasel, D., Gascard, J.C., & Koltermann, K.P. 1987. Large-scale oceanography in Fram Strait during the 1984 Marginal Ice Zone Experiment. *Journal of Geophysical Research*, **92**, 6719–6728.
- Robinson, A.R. 1983. *Eddies in Marine Science*. Springer-Verlag.
- Robinson, I.S. 2004. *Measuring the oceans from space: the principles and methods of satellite oceanography*. Springer-Verlag.
- Sandven, S., Johannessen, O.M., & Johannessen, J.A. 1991. Mesoscale eddies and chimneys in the marginal ice zone. *Journal of Marine Systems*, **2**(1-2), 195–208.
- Shuchman, R.A., Burns, B.A., Johannessen, O.M., Josberger, E.G., Campbell, W.J., Manley, T.O., & Lannelongue, N. 1987. Remote sensing of the Fram Strait marginal ice zone. *Science*, **236**(4800), 429.
- Smith, D.C., & Bird, A.A. 1991. The interaction of an ocean eddy with an ice edge ocean jet in a marginal ice zone. *Journal of Geophysical Research*, **96**(C3), 4675–4689.
- Smith, D.C., Morison, J.H., Johannessen, J.A., & Untersteiner, N. 1984. Topographic generation of an eddy at the edge of the East Greenland current. *Journal of Geophysical Research*, **89**, 8205–8208.
- Spren, G., & Kaleschke, L. 2011 (May). *University of Hamburg, Institute of Oceanography*. <http://www.ifm.zmaw.de/forschung/fernerkundung-assimilation/meereis/amsr-e-ice-concentration>.
- Steele, M., & Flato, G.M. 2000. Sea ice growth, melt and modeling: a survey. *Nato Series 2 Environmental Security*, **70**, 533–588.
- Stoffelen, A., & Anderson, D. 1997. Scatterometer data interpretation: Estimation and validation of the transfer function CMOD4. *Journal of Geophysical Research*, **102**(C3), 5767–5780.
- Taylor, G.I. 1917. Motion of solids in fluids when the flow is not irrotational. *Proceedings of the Royal Society of London. Series A, Containing Papers of a Mathematical and Physical Character*, **93**(648), 99–113.
- Thomas, D.N., & Dieckmann, G.S. 2003. *Sea ice: an introduction to its physics, chemistry, biology and geology*. Blackwell Publishing.

Unden, P., Rontu, L., Järvinen, H., Lynch, P., Calvo, J., Cats, G., Cuxart, J., Eerola, K., Fortelius, C., Garcia-Moya, J.A., *et al.* 2002. HIRLAM-5 scientific documentation.

Vinje, T., & Finnekåsa, Ø. 1986. *The ice transport through the Fram Strait*. Norsk Polarinstitut.